Available online at www.sciencedirect.com
ScienceDirect
Journal of the Mechanics and Physics of Solids 56 (2008) 1852–1884
JOURNAL OF THE MECHANICS AND PHYSICS OF SOLIDS
www.elsevier.com/locate/jmps

Biothermomechanics of skin tissues

F. Xu[a], T.J. Lu[b,*], K.A. Seffen[a]

[a]*Engineering Department, Cambridge University, Cambridge CB2 1PZ, UK*
[b]*MOE Key Laboratory of Strength and Vibration, School of Aerospace, Xi'an Jiaotong University, Xi'an 710049, PR China*

Received 23 March 2007; received in revised form 12 November 2007; accepted 27 November 2007

Abstract

Biothermomechanics of skin is highly interdisciplinary involving bioheat transfer, burn damage, biomechanics and neurophysiology. During heating, thermally induced mechanical stress arises due to the thermal denaturation of collagen, resulting in macroscale shrinkage. Thus, the strain, stress, temperature and thermal pain/damage are highly correlated; in other words, the problem is fully coupled. The aim of this study is to develop a computational approach to examine the heat transfer process and the heat-induced mechanical response, so that the differences among the clinically applied heating modalities can be quantified. Exact solutions for temperature, thermal damage and thermal stress for a single-layer skin model were first derived for different boundary conditions. For multilayer models, numerical simulations using the finite difference method (FDM) and finite element method (FEM) were used to analyze the temperature, burn damage and thermal stress distributions in the skin tissue. The results showed that the thermomechanical behavior of skin tissue is very complex: blood perfusion has little effect on thermal damage but large influence on skin temperature distribution, which, in turn, influences significantly the resulting thermal stress field; the stratum corneum layer, although very thin, has a large effect on the thermomechanical behavior of skin, suggesting that it should be properly accounted for in the modeling of skin thermal stresses; the stress caused by non-uniform temperature distribution in the skin may also contribute to the thermal pain sensation.

Keywords: Skin tissue; Biothermomechanics; Analytical model; Numerical method; Thermal

1. Introduction

Skin, with its three-layer composition of epidermis, dermis and subcutaneous tissue (see Fig. 1a; Whitton and Everall, 1973), is the largest single organ of the body. It plays important roles including sensory roles, thermoregulation and host defense. Thermoregulation is a vital process: skin functions thermally as a heat generator, absorber, transmitter, radiator, conductor and vaporizer. Comprehension of the phenomena of heat transfer and related thermomechanics in soft tissues is of great importance and can contribute to a variety of medical applications. The study of biothermomechanics of skin is highly interdisciplinary, involving bioheat transfer, burn damage, biomechanics and neurophysiology.

*Corresponding author. Tel.: +86 29 82665600; fax: +86 29 83234781.
E-mail address: tjlu@mail.xjtu.edu.cn (T.J. Lu).

0022-5096/$ - see front matter © 2007 Elsevier Ltd. All rights reserved.
doi:10.1016/j.jmps.2007.11.011

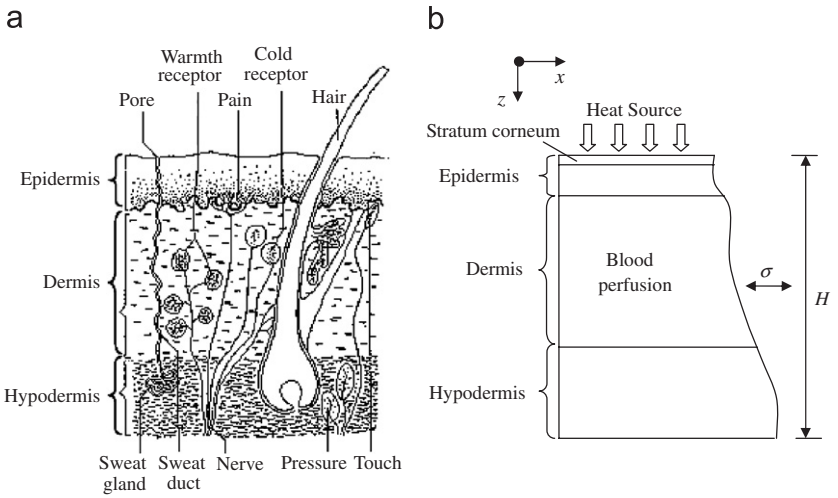

Fig. 1.

1.1. Study of skin thermomechanics is highly cross-disciplinary

Thermal behavior skin tissue, or, heat transfer in skin tissue is mainly a heat conduction process coupled to complicated physiological processes, including blood circulation, sweating, metabolic heat generation, and, sometimes, heat dissipation via hair or fur above the skin surface. The thermal properties of skin vary between different layers; even within the same layer, there exists large non-homogeneity and anisotropy due to the presence of blood vessels. Both the physiological processes and thermal properties of skin are influenced by a variety of factors such as temperature, damage, pressure, age, etc. To complicate matters, skin is an active, self-regulating system: heat transfer through the skin dramatically affects the state of skin, which can lead to the redistribution of skin blood flow over the cutaneous vascular network, whereby influencing the thermal response of the skin tissue. For example, at rest, in a thermally neutral environment, the skin receives 5–10% of the cardiac output, which can increase to 50–70% during severe heat stress or approach zero in a cold environment (Yen and Braverman, 1976); in thermal stress, skin blood flow can rise to levels more than 50-fold its value during thermoregulation (Joyner and Dietz, 1997); at high blood perfusion rate, the amount of blood in the deep dermal plexuses may exceed that of the papillary capillaries by a factor of 30 (Conrad et al., 1971), and in this case local heat transfer in the skin may be dominated by convection of the perfused blood rather than tissue conduction (Hales et al., 1978).

It has been established that skin *in vivo* is mechanically heterogeneous, anisotropic, nonlinear, viscoelastic and under tension. It is affected by many factors such as age, gender, site, hydration, etc. Furthermore, simple elastomeric constitutive models are not suitable to describe the complicated mechanical behavior of skin (Fung, 1990).

The major constituent of dry skin is collagen. During heating, thermally induced mechanical stress appears due to thermal denaturation of collagen, which is macroscopic thermal shrinkage. It has been found that the type of mechanical loading is functionally as important as the temperature level during shrinkage (Chen et al., 1998b). Furthermore, during denaturation, not only the structure, but also the hydration level of collagen changes. Thus, unsurprisingly, thermal denaturation of a collagenous tissue can lead to remarkable changes in the mechanical, thermal, electrical and optical properties and the strain, stress and temperature are highly correlated; in other words, the problem is fully coupled.

Understanding these factors requires study of the mechanisms underlying thermomechanical behavior of skin.

1.2. Applications of skin thermomechanics

With advances in laser, microwave, radio-frequency and similar technologies, a variety of thermal methods have been developed and applied to the treatment of disease/injury involving skin tissue, where the

effectiveness of these treatments is governed by the coupled thermal, mechanical, biological and neural responses of the affected skin tissue and the precise monitoring of the spatial and temporal distribution of temperature, damage and stress in the skin tissue is therefore required. Thus far, improvements in treatment have been obtained largely by empirical methods, leading to elemental progress. Therefore, the proposed research is important and contributes to medical applications for it attempts to understand the macroscale tissue response to heat-induced micro-structural transformations.

A noxious thermal stimulus, hot or cold, applied to human skin is one of the three main causes of pain. Thermally induced damage plays an important role in causing thermal pain and therefore, a better understanding of the temperature distribution, heat transfer process and related thermomechanics in skin contributes to the study of the causes of pain and its relief. Besides biomedical applications, space and military missions may benefit from the proposed study. Extreme environments encountered in space travel and in some military activities make it necessary to provide astronauts and military personnel with sophisticated garments for thermal protection. Challenges are also posed by the need to understand possible thermal effects on military personnel exposed to irradiation.

1.3. Aims and objectives

The objective of this work is to understand the mechanisms underlying bioheat transfer, thermomechanics and thermal pain in skin by using theoretical and numerical methods, and then apply these to special medical treatments. The transfer of heat in soft tissues during thermal therapies will be analyzed in order to model and optimize thermotherapy procedures, and to establish a mathematical thermal pain model to predict thermal pain caused by medical treatment. A computational approach will be established to examine the heat transfer process and heat-induced mechanical response, so that the differences among clinically applied heating modalities can be established.

2. Thermomechanical analysis of skin tissues

2.1. Bioheat transfer

Since the appearance of Pennes' bioheat equation (Pennes, 1948), a variety of models on the heat transfer in different tissues of human body have been proposed, where the body tissue may be represented as a homogeneous continuum material with an embedded hierarchical vascular network (Lubashevsky and Gafiychuk, 2004). According to the different approaches in which the influence of blood flow in the vascular network may be considered, these models can be basically classified into four categories (Arkin et al., 1994; Charny, 1992; Crezee et al., 1994; Khaled and Vafai, 2003; Stanczyk and Telega, 2002): continuum models, vascular models, hybrid models and models based on porous media theory.

The transfer of heat in skin is mainly a heat conduction process, which is coupled to several additional complicated physiological processes, one of the most important being blood perfusion. Since the effect of blood vessels on heat transfer is strongly related to their sizes (Abramson, 1967; Chato, 1980; Lemons et al., 1987; Weinbaum et al., 1984), a thermal equilibration length of blood vessels, L_{eq}, has been introduced to characterize the effects of blood vessels of different sizes on heat transfer. By definition, L_{eq} is the length at which the difference between blood and tissue temperatures decreases to $1/e$ of the initial value ($e = 2.718$ is the exponent). The ratio of thermal equilibration length to actual vessel length ($\varepsilon = L_{\mathrm{eq}}/L$) demonstrates the distinction of thermal significance. If L_{eq} is significantly shorter than the characteristic length of blood vessel, L, blood will exit the vessel at essentially the tissue temperature. If L_{eq} is much larger relative to L, the temperature of blood will not decay and it will leave the tissue at the inflow temperature (Chato, 1980; Chen and Holmes, 1980). Since L_{eq} for typical blood vessels in skin tissue is about 3×10^{-5}–2×10^{-4} mm (Crezee and Lagendijk, 1992), which is considerably shorter than L, blood exits the vessel at approximately the tissue temperature. Consequently, the Pennes equation suffices for modeling skin heat transfer, given as (Pennes, 1948)

$$\rho c \frac{\partial T}{\partial t} = k \frac{\partial^2 T}{\partial z^2} + \varpi_{\mathrm{b}} \rho_{\mathrm{b}} c_{\mathrm{b}} (T_a - T) + q_{\mathrm{met}} + q_{\mathrm{ext}}, \tag{1}$$

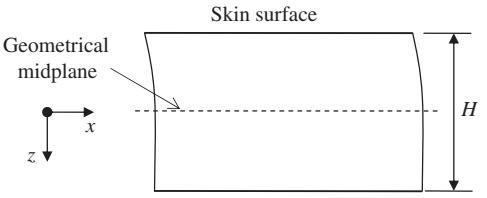

Fig. 2.

where ρ, c and k are the density, specific heat and thermal conductivity of skin tissue, respectively; ρ_b and c_b are the density and specific heat of blood, ϖ_b is the blood perfusion rate; T_a and T are the temperatures of blood and skin tissue, respectively; q_{met} is the metabolic heat generation in the skin tissue and q_{ext} is the heat generated by other heating methods.

In the present study, a one-layer model is proposed first for the theoretical analysis of heat transfer in skin, where the skin is treated as a homogenous medium with constant properties. For simplicity, one-dimensional (1-D) case is studied, as shown in Fig. 2, which is a good approximation when heat mainly propagates in the direction normal to the skin surface (e.g. during laser heating). Later, multi-layer skin models will also be established according to the real skin structure (see Fig. 1b) and solved by numerical methods including finite element method and (FEM) finite difference method (FDM).

2.1.1. Description of the problem

The skin tissue is considered as a perfect, infinitely wide/long plate of thickness, H, according to its anatomical structure, where the Cartesian coordinates are embedded at the center of the plate, as shown in Fig. 2. Initially, the skin tissue has a temperature distribution $T_0(z)$, and at time $t=0$ the skin surface (at $z=-H/2$) is suddenly exposed to a thermal agitation, derived from either a hot contacting plate, a convective medium, or a constant heat flux, whereas on the bottom, $z=H/2$, the surface is held at the core temperature, T_c, or thermally insulated. The effect of blood perfusion is regarded as a heat source under heating (or heat sink under cooling) distributed uniformly inside the tissue. The Pennes equation, as given in Eq. (1), is employed to describe the heat transfer process. Using the following transformation (Deng and Liu, 2002):

$$T(z,t)=T_0(z)+W(z,t)\,e^{-(\varpi_b\rho_b c_b/\rho c)t}. \tag{2}$$

Eq. (1) can be changed to

$$\frac{\partial W}{\partial t}=\alpha\frac{\partial^2 W}{\partial z^2}+\frac{q_{ext}(z,t)+q_{met}(z,t)}{\rho c}e^{-(\varpi_b\rho_b c_b/\rho c)t}, \tag{3}$$

where $\alpha=k/\rho c$ is the thermal diffusivity of the tissue.

In this paper, solutions of Eqs. (1)–(3) under six different kinds of boundary conditions listed below are obtained by using the Green function method (Ozisik, 1993), including two solutions given by Deng and Liu (2002) which are defined by boundary conditions II and III. Since the metabolic heat generation q_{met} is several orders less than that of external heat generation q_{ext} (Gordon et al., 1976), it is neglected in the derivation of the solutions. It should be noted here that this section is investigating wider different boundary conditions for this provides a variety of solutions.

(1) *Boundary condition I:* For this kind of boundary condition, the skin is heated at the surface by a heat source with a constant temperature, T_∞, e.g. in contact with a hot plate, while the bottom of the skin tissue is kept at body temperature, T_c. The boundary condition can be written as

$$\begin{cases} T=T_\infty, & z=-H/2,\\ T=T_c, & z=H/2. \end{cases}$$

The corresponding Green's function is obtained as

$$G(z,t|z',\tau)=\frac{2}{H}\sum_{m=1}^{\infty}\mathrm{e}^{-\alpha\beta_m^2(t-\tau)}\sin(\beta_m z)\sin(\beta_m z'), \tag{4}$$

where $\beta_m=m\pi/H, m=1,2,3,\ldots$. The solution is given by

$$T(z,t)=T_0(z)+\frac{2\alpha}{H}\left[T_\infty-k\left.\frac{\mathrm{d}T_0(z)}{\mathrm{d}z}\right|_{z=0}\right]\times\sum_{m=1}^{\infty}\beta_m\sin[\beta_m(z+H/2)]\frac{1}{\alpha\beta_m^2+\dfrac{\varpi_\mathrm{b}\rho_\mathrm{b}c_\mathrm{b}}{\rho c}}\left(1-\mathrm{e}^{-\alpha\beta_m^2t-(\varpi_\mathrm{b}\rho_\mathrm{b}c_\mathrm{b}/\rho c)t}\right), \tag{5}$$

where $T_0(z)$ is the initial temperature field in the tissue.

(2) *Boundary condition II:* For this kind of boundary condition, the skin surface is heated at a constant heat flux, f_2, e.g. heated by fire, while the bottom of the skin tissue is at body temperature. The boundary condition can be written as

$$\begin{cases}-k\partial T/\partial z=f_2(t), & z=-H/2,\\ T=T_\mathrm{c}, & z=H/2.\end{cases}$$

The corresponding Green's function can be obtained as

$$G_2(z,t|z',\tau)=\frac{2}{H}\sum_{m=1}^{\infty}\mathrm{e}^{-\alpha\beta_m^2(t-\tau)}\cos(\beta_m z)\cos(\beta_m z'). \tag{6}$$

Solution:

$$T(z,t)=T_0(z)+\left[k\left.\frac{\mathrm{d}T_0(z)}{\mathrm{d}z}\right|_{z=0}+f_2(t)\right]\frac{\alpha}{k}\frac{2}{H}\times\sum_{m=1}^{\infty}\cos[\beta_m(z+H/2)]\frac{1}{\alpha\beta_m^2+\dfrac{\varpi_\mathrm{b}\rho_\mathrm{b}c_\mathrm{b}}{\rho c}}\left(1-\mathrm{e}^{-\alpha\beta_m^2t-(\varpi_\mathrm{b}\rho_\mathrm{b}c_\mathrm{b}/\rho c)t}\right), \tag{7}$$

where $\beta_m=(2m-1)/(2H)\pi, m=1,2,3,\ldots$.

(3) *Boundary condition III:* For this kind of boundary condition, the skin surface is heated by a convective heat source of temperature, f_3, with convective heat transfer coefficient h_3, e.g. heated by flowing boiling water, while the bottom of the skin tissue is thermally insulated, e.g. the case of very thick fat layer. The boundary condition can be written as

$$\begin{cases}-k\partial T/\partial z=h_3(f_3-T), & z=-H/2,\\ T=T_\mathrm{c}, & z=H/2.\end{cases}$$

The corresponding Green's function can be obtained as

$$G_3(z,t|z',\tau)=\frac{2\left[\beta_m^2+(h_3/k)^2\right]}{H[\beta_m^2+(h_3/k)^2]+(h_3/k)}\sum_{m=1}^{\infty}\mathrm{e}^{-\alpha\beta_m^2(t-\tau)}\sin[\beta_m(H-z)]\sin[\beta_m(H-z')]. \tag{8}$$

Solution:

$$T(z,t) = T_0(z) + \frac{\alpha}{k} h_3 \left[\frac{k}{h_3} \left. \frac{\mathrm{d}T_0(z)}{\mathrm{d}z} \right|_{z=0} - T_0(z)|_{z=0} + f_3(t) \right] \times \sum_{m=1}^{\infty} \left\{ \begin{array}{l} \left(\dfrac{2[\beta_m^2 + (h_3/k)^2]}{H[\beta_m^2 + (h_3/k)^2] + h_3/k} \sin[\beta_m(H/2 - z)] \sin(\beta_m H) \right) \\ \dfrac{1}{\alpha\beta_m^2 + \dfrac{\varpi_\mathrm{b}\rho_\mathrm{b}c_\mathrm{b}}{\rho c}} \left(1 - \mathrm{e}^{-\alpha\beta_m^2 t - (\varpi_\mathrm{h}\rho_\mathrm{b}c_\mathrm{b}/\rho c)t} \right) \end{array} \right\}, \tag{9}$$

where β_m is the positive roots of $\beta_m \cot(\beta_m H) = -h_3/k$.

(4) *Boundary condition IV:* For this kind of boundary condition, the skin is heated at the surface by a heat source with a constant temperature, T_∞, while the bottom of the skin tissue is thermally insulated. The boundary condition can be written as

$$\begin{cases} T = T_\infty, & z = -H/2, \\ \partial T/\partial z = 0, & z = H/2. \end{cases}$$

Solution:

$$T(z,t) = T_0(z) + \frac{2\alpha}{H}(T_\infty - T_0) \sum_{m=1}^{\infty} \beta_m \sin(\beta_m z) \frac{1}{\alpha\beta_m^2 + \dfrac{\varpi_\mathrm{b}\rho_\mathrm{b}c_\mathrm{b}}{\rho c}} \left(1 - \mathrm{e}^{-\alpha\beta_m^2 t - (\varpi_\mathrm{b}\rho_\mathrm{b}c_\mathrm{b}/\rho c)t} \right), \tag{10}$$

where $\beta_m = (2m-1)/(2H)\pi, m = 1, 2, 3, \ldots$.

(5) *Boundary condition V:* For this kind of boundary condition, the skin surface is heated at a constant heat flux, f_5, while the bottom of the skin tissue is thermally insulated. The boundary condition can be written as

$$\begin{cases} -k\partial T/\partial z = f_5(t), & z = -H/2, \\ \partial T/\partial z = 0, & z = H/2. \end{cases}$$

Solution:

$$T(z,t) = T_0(z) + \left[k \left. \frac{\mathrm{d}T_0(z)}{\mathrm{d}z} \right|_{z=0} + f_5(t) \right] \frac{\alpha}{k} \frac{2}{H} \times \left\{ \begin{array}{l} \dfrac{\rho c}{\varpi_\mathrm{b}\rho_\mathrm{b}c_\mathrm{b}} (1 - \mathrm{e}^{-(\varpi_\mathrm{b}\rho_\mathrm{b}c_\mathrm{b}/\rho c)t}) \\ + \displaystyle\sum_{m=2}^{\infty} \cos[\beta_m(z + H/2)] \frac{1}{\alpha\beta_m^2 + \dfrac{\varpi_\mathrm{b}\rho_\mathrm{b}c_\mathrm{b}}{\rho c}} (1 - \mathrm{e}^{-\alpha\beta_m^2 t - (\varpi_\mathrm{b}\rho_\mathrm{b}c_\mathrm{b}/\rho c)t}) \end{array} \right\}, \tag{11}$$

where $\beta_m = (m-1)/(H)\pi, m = 2, 3, 4, \ldots$.

(6) *Boundary condition VI:* For this kind of boundary condition, the skin surface is heated by a convective heat source of temperature, f_6, with convective heat transfer coefficient h_6, while the bottom of the skin tissue is thermally insulated. The boundary condition can be written as

$$\begin{cases} -k\partial T/\partial z = h_f(f_6 - T), & z = -H/2, \\ T = T_\mathrm{c}, & z = H/2. \end{cases}$$

Solution:

$$T(z,t) = T_0(z) + \frac{\alpha}{k} h_6 \left[\frac{k}{h_6} \frac{dT_0(z)}{dz}\bigg|_{z=0} - T_0(z)\big|_{z=0} + f_6(t) \right] \times \sum_{m=1}^{\infty} \left\{ \frac{2[\beta_m^2 + (h_6/k)^2]}{H[\beta_m^2 + (h_6/k)^2] + h_6/k} \cos[\beta_m(H/2 - z)] \cos(\beta_m H) \times \frac{1}{\alpha\beta_m^2 + \frac{\varpi_b \rho_b c_b}{\rho c}} \left(1 - e^{-\alpha\beta_m^2 t - (\varpi_b \rho_b c_b/\rho c)t}\right) \right\}, \tag{12}$$

where β_m is the positive roots of $\beta_m \tan(\beta_m H) = h_6/k$.

2.2. Skin heat transfer model considering hair or fur

Due to the high surface-mass ratio and the dense distribution of blood vessels within skin tissues, skin appendages (such as hair/fur and sweat glands) play significant roles in thermoregulation. In some situations, the hair strands are so dense that they can trap a layer of air and thus work as an insulation layer (Gebremedhin and Wu, 2001): for example, it was found in dairy cows that air occupies 90% of the surface layer volume and hairs occupy just 10% (Arkin et al., 1991). Since the thermal conductivity of hair is about 14 times greater than that of air (about 0.37Ẇ/mK for human hair and 0.026 W/mK for air), every single hair strand also works as fin, which enhances the heat transfer from the skin and thus is an unwanted effect in the thermal insulation sense due to the heat loss (Bejan, 1990a, b; Gebremedhin and Wu, 2001).

Most studies in this area concern the effective cooling of animals, especially livestock, in hot environments (Gebremedhin and Wu, 2001, 2002). Theoretically, Bejan (1990a, b) analyzed the fundamental mechanism of heat transfer through a surface covered with perpendicular hair strands of uniform density, where the skin was treated as a medium with isothermal surface. Through the analysis, it was found that when the velocity of air flow through the space between hairs is small enough and thus conforms to the Darcy regime, there exists an optimum hair strand diameter for minimum total heat loss.

Fig. 3 shows schematically the trapped air–hair layer model. With the methods of Bejan (1990a; b) and Gebremedhin and Wu (2001), a 1-D model of skin heat transfer is developed below.

The density of hair strands is given by n, where

$$n = \frac{\text{number of strands of hair}}{\text{unit area of skin surface}}, \tag{13}$$

which is assumed to be a constant for it varies little over a small skin area. Denoting A_s as the cross-sectional area of one hair strand, the porosity of the region above the skin is defined to be ϕ, equal to

$$\Phi = \frac{\text{air volume}}{\text{total volume}} = 1 - nA_s. \tag{14}$$

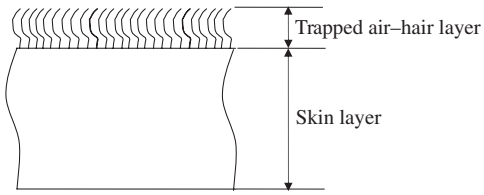

Fig. 3.

The heat transfer in the air–hair layer in Fig. 3 is governed by

$$(\rho c)_{\text{eff}} \frac{\partial T}{\partial t} = k_{\text{eff}} \nabla^2 T, \tag{15}$$

where T is the temperature, ρ is the density and c is the specific heat. Since (ρc) has a physical meaning of heat capacity, which is the measure of the heat energy required to increase the temperature of an object by a certain temperature interval, the following relation can be obtained according to the energy conservation:

$$(\rho c)_{\text{eff}} = (\rho c)_{\text{air}} \phi + (\rho c)_{\text{hair}} (1 - \phi). \tag{16}$$

In view of it large density, e.g. the average human scalp measures approximately $770/\text{cm}^2$ (Schwartz and Rosenblum, 1981), the air–hair layer treated as an orthotropic material, or in other words, it is regarded as uniform on the plane parallel to the skin surface. Its effective thermal conductivity k_{eff} may be defined as

$$k_{\text{eff}} = 0.5(k_z + k_x), \tag{17}$$

$$k_z = nA_s k_h + (1 - nA_s)k_a = (1 - \phi)k_h + \phi k_a, \quad k_y = \frac{k_a(l_c - d_h)}{l_c} + \frac{d_h k_a k_h}{d_h k_a + (1_c - d_h)k_h}, \tag{18}$$

where the coordinate z denotes the skin thickness direction, x denotes the direction parallel to the skin surface; $l_c = 1/\sqrt{n}$; d_h is the diameter of hair strand; k_a is the thermal conductivity of air and is assumed

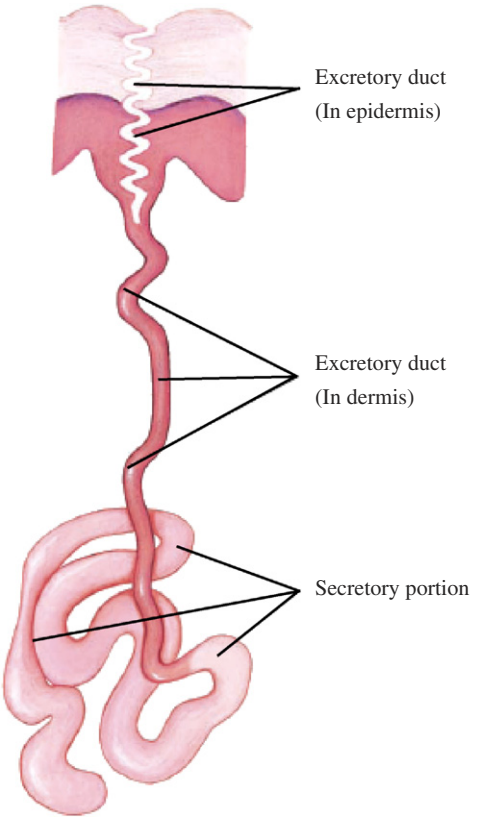

Fig. 4.

to be 0.025 W/m K; k_h is the thermal conductivity of hair strand, where $k_f \approx 10k_a$ assumed from known data.

2.3. Skin heat transfer model considering sweating

Under normal conditions, in general, heat is lost from the body through skin in two ways: insensible perspiration (perspiration that evaporates before it is perceived as moisture on the skin) due to the continuous leeching of fluid from the capillaries of the deeper layers of the skin to its dry surface, and sweat vaporization from the skin surface which decreases its temperature. Thus, sweating contributes significantly to the thermoregulation of skin.

The sweat gland is a simple, highly coiled, tubular gland, as shown in Fig. 4 (Eroschenko, 2004). In general, it extends deep into the dermis and is composed of three regions: the secretory portion, which is the coiled region of the sweat gland and located in the dermis; the excretory duct, which leaves the secretory region of the sweat gland and straightens out to the epidermis; the spiral course in the epidermis, which passes through the epidermal cells to the skin surface.

With the heat pipe theory to model the eccrine sweat gland[1] (Reay and Thiele, 1977), a theoretical model is developed.

(1) *Consideration of latent sweat*: For latent sweat, in the secretory portion, the sweat absorbs heat and changes to vapor, which flows along the straight dermal duct into the superficial layer of the skin where, due to the low pressure and low temperature, it releases the heat and changes to fluid in the spiraled duct, see Fig. 4. Following Liu and Wang (1997), the flow of sweat in the skin is treated as a flow in a porous medium, so that the thermal influence of sweat on skin heat transfer can be considered as

For epidermis:

$$\rho c\frac{\partial T}{\partial t} = k\nabla^2 T - \rho_s c_s \overline{V}\nabla T + q_s. \tag{19}$$

For dermis:

$$\rho c\frac{\partial T}{\partial t} = k\nabla^2 T + \varpi_b \rho_b c_b (T_a - T) + q_{met}. \tag{20}$$

For subcutaneous fat:

$$\rho c\frac{\partial T}{\partial t} = k\nabla^2 T + \varpi_b \rho_b c_b (T_a - T) + q_{met}, \tag{21}$$

where ϖ_b is the blood perfusion rate; T_a and T are the temperatures of blood and skin tissue, respectively; q_{met} is the metabolic heat generation in the skin tissue; ρ is the density and c is the specific heat; q_s is the heat which the sweat absorbs in secretary portion and releases in the spiralled duct; q_{met} is the metabolic heat generation; $-\rho_s c_s \overline{V}\nabla T$ is the convective heat transfer of sweat with skin and $\overline{V}$ is velocity of sweat in the duct.

(2) *Consideration of sensible sweat:* For sensible sweat, the sweat flows into the skin surface and then evaporates. Its influence on skin heat transfer can be modeled as

For epidermis:

$$\rho c\frac{\partial T}{\partial t} = k\nabla^2 T - \rho_s c_s \overline{V}\nabla T. \tag{22}$$

For dermis:

$$\rho c\frac{\partial T}{\partial t} = k\nabla^2 T + \varpi_b \rho_b c_b (T_a - T) + q_{met} - \rho_s c_s \overline{V}\nabla T. \tag{23}$$

For subcutaneous fat:

$$\rho c\frac{\partial T}{\partial t} = k\nabla^2 T + \varpi_b \rho_b c_b (T_a - T) + q_{met}. \tag{24}$$

[1] In humans, there are four kinds of sweat glands which differ greatly in both the composition of the sweat and its purpose, where the normal sweat used in temperature control is through eccrine glands.

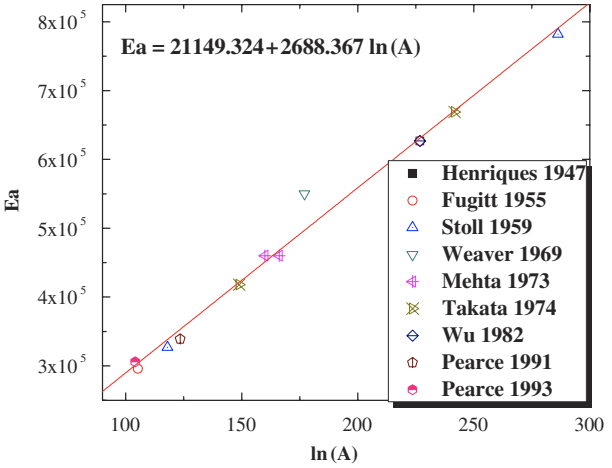

Fig. 5.

2.4. Thermal damage (denaturation)

The pioneering Arrhenius burn model proposed by Henriques and Moritz (1947) and Moritz and Henriques (1947) is widely used. They proposed that skin damage could be represented as a chemical rate process, which could be calculated by using a first order Arrhenius rate equation, whereby damage is related to the rate of protein denaturation (κ) and exposure time (τ) at a given absolute temperature (T). The measure of thermal injury Ω was introduced and its rate κ was postulated to satisfy:

$$\kappa(T) = \mathrm{d}\Omega/\mathrm{d}\tau = A\,\exp(-E_a/RT) \tag{25}$$

or, equivalently

$$\Omega = \int_0^t A\exp(-E_a/RT)\,\mathrm{d}t, \tag{26}$$

where A is a material parameter equivalent to a frequency factor, E_a is the activation energy, and $R = 8.314\,\mathrm{J/mol\,K}$ is the universal gas constant. Eq. (25) indicates that a reaction proceeds faster with larger values of T or A for the same E_a, or with smaller values of E_a for the same A. The constants A and E_a are obtained experimentally.

Many researchers have proposed other models, but most of them have similar format, where the only differences are in the coefficients used in the burn damage integral, arising from the different experimental databases used to define the models and the different emphasis when analyzing the burn process. The available Arrhenius parameters (A, E_a) used to calculate thermal damage for skin tissue from the literature has been reviewed, and is fitted with the method used by Wright (2003), as shown in Fig. 5. The results of Fig. 5 clearly suggest a linear relationship after a least-square fit between the Arrhenius parameters for skin tissue, given by

$$E_a = 21149.324 + 2688.367\,\ln(A). \tag{27}$$

With the above relation, the reaction rate of the thermal damage process follows as

$$\kappa(T) = \exp[(E_a - 21149.324)/2688.367]\exp(-E_a/RT). \tag{28}$$

If the temperature is a constant and E_a is specified, the thermal damage can be calculated by:

$$\Omega = \int_0^t k(T)\,\mathrm{d}t = k(T)t. \tag{29}$$

Assuming $\Omega = 1.0$ denotes the beginning of irreversible damage, we can calculate the time for the appearance of irreversible damage at temperature T, as

$$t_{\Omega-1} = 1/k(T) = 1/(\exp[(E_a - 21149.324)2688.367]\,\exp(-E_a RT)). \tag{30}$$

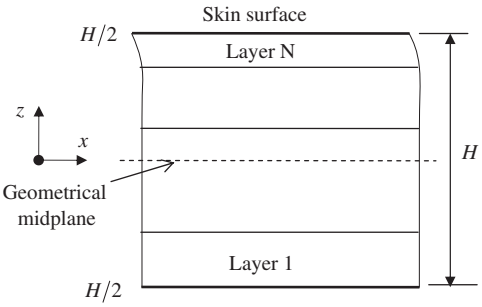

Fig. 6.

2.5. Thermal stresses

As previously discussed, skin has a complicated multi-layer structure (see Fig. 1a). Whilst the thermal properties of the layers have the same order of magnitude, see Table 2, so that a one-layer continuum model for heat transfer may be assumed, the mechanical properties vary greatly by up to three orders of magnitude from one layer to another (see Table 3). Consequently, in order to obtain the distribution of heat-induced stresses, the skin must be treated as a laminated composite structure, with each layer assumed to be uniform with linear, orthotropic thermoelastic properties, as shown in Fig. 6. The thermomechanical behavior of skin tissue is simplified to be a 'sequentially coupled' problem, in other words, the mechanical behavior has no influence on thermal behavior and vice versa. The temperature field in skin tissue is first obtained from solving the governing equations of biological heat transfer, which is then used as the input to the thermomechanical model, from which the corresponding thermal stress field is obtained.

For the general case of multiple layers, each having a thickness, t_k, and material properties of Young's modulus, E_k and poisson ratio, v_k, where $k = 1, 2, \ldots, N$ with N being total number of layers, the in-plane extensional, coupling and bending stiffnesses of the overall laminate of structure are given by, respectively (Kollar and Springer, 2003):

$$A_{ij} = \sum_{k=1}^{N} (\overline{Q}_{ij})_k (z_k - z_{k-1}); \quad B_{ij} = \frac{1}{2} \sum_{k=1}^{N} (\overline{Q}_{ij})_k (z_k^2 - z_{k-1}^2); \quad D_{ij} = \frac{1}{3} \sum_{k=1}^{N} (\overline{Q}_{ij})_k (z_k^3 - z_{k-1}^3), \tag{31}$$

where A_{ij}, B_{ij} and D_{ij} are separately assembled into the elements of stiffness matrices $[A]$, $[B]$ and $[D]$; $[\overline{Q}]$ is the stiffness matrix of the layered skin structure, defined by:

$$[\overline{Q}] = \begin{bmatrix} \overline{Q}_{11} & \overline{Q}_{12} & \overline{Q}_{16} \\ \overline{Q}_{12} & \overline{Q}_{22} & \overline{Q}_{26} \\ \overline{Q}_{16} & \overline{Q}_{26} & \overline{Q}_{66} \end{bmatrix}, \quad \begin{cases} (\overline{Q}_{11})_k = (\overline{Q}_{22})_k = E_k/(1 - v_k^2); \ (\overline{Q}_{16})_k = (\overline{Q}_{26})_k = 0, \\ (\overline{Q}_{12})_k = v_k E_k/(1 - v_k^2); \ (\overline{Q}_{66})_k = E_k/[2(1 + v_k)]. \end{cases} \tag{32}$$

Due to the combined thermal and mechanical loading, the vector of strains, ε_k, at a point in each layer under plane-strain conditions are

$$\{\varepsilon\}_k = [\overline{S}]_k \{\sigma\}_k + \{\lambda\}_k \Delta T, \tag{33}$$

where ΔT is the temperature difference at a point relative to a reference temperature, λ is the vector of the thermal expansion coefficient and $[\overline{S}]_k$ is the stiffness matrix.

By inverting the above equation, the vector of stresses, σ_k, can be obtained as

$$\{\sigma\}_k = [\overline{Q}]_k [\{\varepsilon\}_k - \{\lambda\}_k \Delta t]. \tag{34}$$

In a lamina, the total strains over the whole depth generally do not vanish, but given as

$$\{\varepsilon\}_k = \{\varepsilon^0\} + z\{\kappa\}. \tag{35}$$

Where $\{\varepsilon^0\}$ and $\{\kappa\}$ are the strain and curvature at the geometrical midplane. The resulting stresses are

$$\{\sigma\}_k = [\overline{Q}]_k(\{\varepsilon^0\} + z\{\kappa\} - \{\lambda\}_k \Delta T), \tag{36}$$

whilst the resultant laminate forces per unit length are found by integrating through the thickness of the laminate

$$\begin{aligned}\{N\} &= \int \{\sigma\}_k \,\mathrm{d}z = \int [\overline{Q}]_k(\{\varepsilon^0\} + z\{\kappa\} - \{\lambda\}_k \Delta T)\,\mathrm{d}z,\\ &= [A]\{\varepsilon^0\} + [B]\{\kappa\} - \{N^{\mathrm{T}}\},\end{aligned} \tag{37}$$

where

$$[A] = \begin{bmatrix} A_{11} & A_{12} & A_{16} \\ A_{12} & A_{22} & A_{26} \\ A_{16} & A_{26} & A_{66} \end{bmatrix}, \quad [B] = \begin{bmatrix} B_{11} & B_{12} & B_{16} \\ B_{12} & B_{22} & B_{26} \\ B_{16} & B_{26} & B_{66} \end{bmatrix} \quad \text{and} \quad \{N^{\mathrm{T}}\} = \int [\overline{Q}]_k \{\lambda\}_k \Delta T \,\mathrm{d}z.$$

Similarly, the resultant moments per unit length are

$$\begin{aligned}\{M\} &= \int \{\sigma\}_k z \,\mathrm{d}z = \int [\overline{Q}]_k(\{\varepsilon^0\} + z\{\kappa\} - \{\lambda\}_k \Delta T) z \,\mathrm{d}z,\\ &= [B]\{\varepsilon^0\} + [D]\{\kappa\} - \{M^{\mathrm{T}}\},\end{aligned} \tag{38}$$

where

$$[D] = \begin{bmatrix} D_{11} & D_{12} & D_{16} \\ D_{12} & D_{22} & D_{26} \\ D_{16} & D_{26} & D_{66} \end{bmatrix}$$

and

$$\{M^{\mathrm{T}}\} = \int [\overline{Q}]_k \{\lambda\}_k \Delta T \,\mathrm{d}z.$$

From Eqs. (37) and (38), we can find

$$\begin{cases} \{N\} + \{N^T\} = [A]\{\varepsilon^0\} + [B]\{\kappa\} \\ \{M\} + \{M^T\} = [B]\{\varepsilon^0\} + [D]\{\kappa\} \end{cases} \Rightarrow \begin{Bmatrix} \varepsilon^0 \\ \kappa \end{Bmatrix} = \begin{Bmatrix} A' & B' \\ B' & D' \end{Bmatrix} \begin{Bmatrix} N^E \\ M^E \end{Bmatrix} \Rightarrow \begin{cases} \varepsilon^0 = A'N^E + B'M^E, \\ \kappa = B'N^E + D'M^E, \end{cases} \tag{39}$$

where

$$\begin{cases} \{N^E\} = \{N\} + \{N^{\mathrm{T}}\}, \\ \{M^E\} = \{M\} + \{M^{\mathrm{T}}\}, \end{cases} \quad \begin{cases} [A'] = [A^*] - [B^*][D^*]^{-1}[C^*] = \begin{bmatrix} a'_{11} & a'_{12} & 0 \\ a'_{12} & a'_{11} & 0 \\ 0 & 0 & a'_{66} \end{bmatrix}, \\ [B'] = [B^*][D^*]^{-1} = \begin{bmatrix} b'_{11} & b'_{12} & 0 \\ b'_{12} & b'_{11} & 0 \\ 0 & 0 & b'_{66} \end{bmatrix}, \end{cases}$$

$$\begin{cases} [C'] = [B'] = \begin{bmatrix} C'_{11} & c'_{12} & 0 \\ c'_{12} & c'_{11} & 0 \\ 0 & 0 & c'_{66} \end{bmatrix}, \\ [D'] = [D^*]^{-1} = \begin{bmatrix} d'_{11} & d'_{12} & 0 \\ d'_{12} & d'_{11} & 0 \\ 0 & 0 & d'_{66} \end{bmatrix}, \end{cases} \quad \begin{cases} [A^*] = [A]^{-1}, \\ [B^*] = -[A]^{-1}[B], \\ [C^*] = [B][A]^{-1}, \\ [D^*] = [D] - [B][A]^{-1}[B]. \end{cases}$$

Thus, the in-plane stresses parallel to the skin surface in each layer (Fig. 6) can be obtained as

$$\{\sigma_{xx}\}_k = \overline{E}_k \left\{ \begin{array}{l} -\overline{\lambda}_k \Delta T + \left[\begin{array}{l} (a'_{11} + a'_{12})(1+v_k)\left(\sum_{i-1}^{M} \int_{z_{i-1}}^{z_i} \overline{E}_i \overline{\lambda}_i \Delta T \, \mathrm{d}z \right) \\ +(b'_{11} + b'_{12})(1+v_k)\left(\sum_{i=1}^{M} \int_{z_{i-1}}^{z_i} \overline{E}_i \overline{\lambda}_i \Delta T z \, \mathrm{d}z \right) \end{array} \right] \\ +z(1+v_k) \left[\begin{array}{l} (b'_{11} + b'_{12}\left(\sum_{i=1}^{M} \int_{z_{i-1}}^{z_i} \overline{E}_i \overline{\lambda}_i \Delta T \, \mathrm{d}z \right) \\ +(d'_{11} + d'_{12})(1+v_k)\left(\sum_{i=1}^{z_i} \int_{z_{i-1}}^{z} \overline{E}_i \overline{\lambda}_i \Delta T z \, \mathrm{d}z \right) \end{array} \right] \end{array} \right\}, \tag{40}$$

where $\overline{E} = E/(1-v^2)$ and $\overline{\lambda} = (1+v)\lambda$.

Eq. (40) has been applied to one-layer, two-layer, three-layer and four-layer skin models and the results are given below.

(1) *For one-layer model:*

$$\sigma_{xx}(x,t) = -\overline{E}\overline{\lambda}(T - T_0) + \frac{\overline{E}\overline{\lambda}}{H} \int_{-H/2}^{H/2} (T - T_0) \, \mathrm{d}z + \overline{E}\overline{\lambda} \frac{12x}{H} \int_{-H/2}^{H/2} (T - T_0) z \, \mathrm{d}z. \tag{41}$$

(2) *For two-layer model (epidermis and dermis):*

$$\sigma_{xx} = \overline{E}_{\mathrm{d}}(1+v_{\mathrm{d}}) \left\{ \begin{array}{l} \left[\begin{array}{l} (a'_{11} + a'_{12})(\int_{z_0}^{z_1} \overline{E}_{\mathrm{d}} \overline{\lambda}_{\mathrm{d}} \Delta T \, \mathrm{d}z + \int_{z_1}^{z_2} \overline{E}_{\mathrm{e}} \overline{\lambda}_{\mathrm{e}} \Delta T \, \mathrm{d}z) \\ (b'_{11} + b'_{12})(\int_{z_0}^{z_1} \overline{E}_{\mathrm{d}} \overline{\lambda}_{\mathrm{d}} \Delta T z \, \mathrm{d}z + \int_{z_1}^{z_2} \overline{E}_{\mathrm{e}} \overline{\lambda}_{\mathrm{e}} \Delta T z \, \mathrm{d}z) \end{array} \right] \\ +z \left[\begin{array}{l} (b'_{11} + b'_{12})(\int_{z_0}^{z_1} \overline{E}_{\mathrm{d}} \overline{\lambda}_{\mathrm{d}} \Delta T \, \mathrm{d}z + \int_{z_1}^{z_2} \overline{E}_{\mathrm{e}} \overline{\lambda}_{\mathrm{e}} \Delta T \, \mathrm{d}z) + \\ (d'_{11} + d'_{12})(\int_{z_0}^{z_1} \overline{E}_{\mathrm{d}} \overline{\lambda}_{\mathrm{d}} \Delta T z \, \mathrm{d}z + \int_{z_1}^{z_2} \overline{E}_{\mathrm{e}} \overline{\lambda}_{\mathrm{e}} \Delta T z \, \mathrm{d}z) \end{array} \right] - \lambda_{\mathrm{d}} \Delta T \end{array} \right\}$$

$$z_0 \leqslant z < z_1 \quad \text{epidermis layer}, \tag{42}$$

$$\sigma_{xx} = \overline{E}_{\mathrm{e}}(1+v_{\mathrm{e}}) \left\{ \begin{array}{l} \left[\begin{array}{l} (a'_{11} + a'_{12})\left(\int_{z_0}^{z_1} \overline{E}_{\mathrm{d}} \overline{\lambda}_{\mathrm{d}} \Delta T \, \mathrm{d}z + \int_{z_1}^{z_2} \overline{E}_{\mathrm{e}} \overline{\lambda}_{\mathrm{e}} \Delta T \, \mathrm{d}z \right) + \\ (b'_{11} + b'_{12})\left(\int_{z_0}^{z_1} \overline{E}_{\mathrm{d}} \overline{\lambda}_{\mathrm{d}} \Delta T z \, \mathrm{d}z + \int_{z_1}^{z_2} \overline{E}_{\mathrm{e}} \overline{\lambda}_{\mathrm{e}} \Delta T z \, \mathrm{d}z \right) \end{array} \right] \\ +z \left[\begin{array}{l} (b'_{11} + b'_{12})\left(\int_{z_0}^{z_1} \overline{E}_{\mathrm{d}} \overline{\lambda}_{\mathrm{d}} \Delta T \, \mathrm{d}z + \int_{z_1}^{z_2} \overline{E}_{\mathrm{e}} \overline{\lambda}_{\mathrm{e}} \Delta T \, \mathrm{d}z \right) + \\ (d'_{11} + d'_{12})\left(\int_{z_0}^{z_1} \overline{E}_{\mathrm{d}} \overline{\lambda}_{\mathrm{d}} \Delta T z \, \mathrm{d}z + \int_{z_1}^{z_2} \overline{E}_{\mathrm{e}} \overline{\lambda}_{\mathrm{e}} \Delta T z \, \mathrm{d}z \right) \end{array} \right] - \lambda_{\mathrm{e}} \Delta T \end{array} \right\}$$

$$z_1 \leqslant z < z_2 \quad \text{dermis layer}. \tag{43}$$

(3) *For three-layer model (epidermis, dermis and fat):*

$$\sigma_{xx}=(1+v_{\mathrm{f}})\overline{E}_{\mathrm{f}}\left\{\begin{array}{l}\left[\begin{array}{l}(a'_{11}+a'_{12})\left(\int_{z_0}^{z_1}\overline{E}_{\mathrm{f}}\overline{\lambda}_{\mathrm{f}}\,\Delta T\,\mathrm{d}z+\int_{z_1}^{z_2}\overline{E}_{\mathrm{d}}\overline{\lambda}_{\mathrm{d}}\,\Delta T\,\mathrm{d}z+\int_{z_2}^{z_3}\overline{E}_{\mathrm{e}}\overline{\lambda}_{\mathrm{e}}\,\Delta T\,\mathrm{d}z\right)\\+(b'_{11}+b'_{12})\left(\int_{z_0}^{z_1}\overline{E}_{\mathrm{f}}\overline{\lambda}_{\mathrm{f}}\,\Delta Tz\,\mathrm{d}z+\int_{z_1}^{z_2}\overline{E}_{\mathrm{d}}\overline{\lambda}_{\mathrm{d}}\,\Delta Tz\,\mathrm{d}z+\int_{z_2}^{z_3}\overline{E}_{\mathrm{e}}\overline{\lambda}_{\mathrm{e}}\,\Delta Tz\,\mathrm{d}z\right)\end{array}\right]\\+z\left[\begin{array}{l}(b'_{11}+b'_{12})\left(\int_{z_0}^{z_1}\overline{E}_{\mathrm{f}}\overline{\lambda}_{\mathrm{f}}\,\Delta T\,\mathrm{d}z+\int_{z_1}^{z_2}\overline{E}_{\mathrm{d}}\overline{\lambda}_{\mathrm{d}}\,\Delta T\,\mathrm{d}z+\int_{z_2}^{z_3}\overline{E}_{\mathrm{e}}\overline{\lambda}_{\mathrm{e}}\,\Delta T\,\mathrm{d}z\right)\\+(d'_{11}+d'_{12})\left(\int_{z_0}^{z_1}\overline{E}_{\mathrm{f}}\overline{\lambda}_{\mathrm{f}}\,\Delta Tz\,\mathrm{d}z+\int_{z_1}^{z_2}\overline{E}_{\mathrm{d}}\overline{\lambda}_{\mathrm{d}}\,\Delta Tz\,\mathrm{d}z+\int_{z_2}^{z_3}\overline{E}_{\mathrm{e}}\overline{\lambda}_{\mathrm{e}}\,\Delta Tz\,\mathrm{d}z\right)\end{array}\right]-\lambda_{\mathrm{f}}\,\Delta T\end{array}\right\}$$

$z_0\leqslant z<z_1$ fat layer, (44)

$$\sigma_{xx}=(1+v_{\mathrm{d}})\overline{E}_{\mathrm{d}}\left\{\begin{array}{l}\left[\begin{array}{l}(a'_{11}+a'_{12})\left(\int_{z_0}^{z_1}\overline{E}_{\mathrm{f}}\overline{\lambda}_{\mathrm{f}}\,\Delta T\,\mathrm{d}z+\int_{z_1}^{z_2}\overline{E}_{\mathrm{d}}\overline{\lambda}_{\mathrm{d}}\,\Delta T\,\mathrm{d}z+\int_{z_2}^{z_3}\overline{E}_{\mathrm{e}}\overline{\lambda}_{\mathrm{e}}\,\Delta T\,\mathrm{d}z\right)\\+(b'_{11}+b'_{12})\left(\int_{z_0}^{z_1}\overline{E}_{\mathrm{f}}\overline{\lambda}_{\mathrm{f}}\,\Delta Tz\,\mathrm{d}z+\int_{z_1}^{z_2}\overline{E}_{\mathrm{d}}\overline{\lambda}_{\mathrm{d}}\,\Delta Tz\,\mathrm{d}z+\int_{z_2}^{z_3}\overline{E}_{\mathrm{e}}\overline{\lambda}_{\mathrm{e}}\,\Delta Tz\,\mathrm{d}z\right)\end{array}\right]\\+z\left[\begin{array}{l}(b'_{11}+b'_{12})\left(\int_{z_0}^{z_1}\overline{E}_{\mathrm{f}}\overline{\lambda}_{\mathrm{f}}\,\Delta T\,\mathrm{d}z+\int_{z_1}^{z_2}\overline{E}_{\mathrm{d}}\overline{\lambda}_{\mathrm{d}}\,\Delta T\,\mathrm{d}z+\int_{z_2}^{z_3}\overline{E}_{\mathrm{e}}\overline{\lambda}_{\mathrm{e}}\,\Delta T\,\mathrm{d}z\right)\\+(d'_{11}+d'_{12})\left(\int_{z_0}^{z_1}\overline{E}_{\mathrm{f}}\overline{\lambda}_{\mathrm{f}}\,\Delta Tz\,\mathrm{d}z+\int_{z_1}^{z_2}\overline{E}_{\mathrm{d}}\overline{\lambda}_{\mathrm{d}}\,\Delta Tz\,\mathrm{d}z+\int_{z_2}^{z_3}\overline{E}_{\mathrm{e}}\overline{\lambda}_{\mathrm{e}}\,\Delta Tz\,\mathrm{d}z\right)\end{array}\right]-\lambda_{\mathrm{d}}\,\Delta T\end{array}\right\}$$

$z_1\leqslant z<z_2$ dermis layer, (45)

$$\sigma_{xx}=(1+v_{\mathrm{e}})\overline{E}_{\mathrm{e}}\left\{\begin{array}{l}\left[\begin{array}{l}(a'_{11}+a'_{12})\left(\int_{z_0}^{z_1}\overline{E}_{\mathrm{f}}\overline{\lambda}_{\mathrm{f}}\,\Delta T\,\mathrm{d}z+\int_{z_1}^{z_2}\overline{E}_{\mathrm{d}}\overline{\lambda}_{\mathrm{d}}\,\Delta T\,\mathrm{d}z+\int_{z_2}^{z_3}\overline{E}_{\mathrm{e}}\overline{\lambda}_{\mathrm{e}}\,\Delta T\,\mathrm{d}z\right)\\+(b'_{11}+b'_{12})\left(\int_{z_0}^{z_1}\overline{E}_{\mathrm{f}}\overline{\lambda}_{\mathrm{f}}\,\Delta Tz\,\mathrm{d}z+\int_{z_1}^{z_2}\overline{E}_{\mathrm{d}}\overline{\lambda}_{\mathrm{d}}\,\Delta Tz\,\mathrm{d}z+\int_{z_2}^{z_3}\overline{E}_{\mathrm{e}}\overline{\lambda}_{\mathrm{e}}\,\Delta Tz\,\mathrm{d}z\right)\end{array}\right]\\+z\left[\begin{array}{l}(b'_{11}+b'_{12})\left(\int_{z_0}^{z_1}\overline{E}_{\mathrm{f}}\overline{\lambda}_{\mathrm{f}}\,\Delta T\,\mathrm{d}z+\int_{z_1}^{z_2}\overline{E}_{\mathrm{d}}\overline{\lambda}_{\mathrm{d}}\,\Delta T\,\mathrm{d}z+\int_{z_2}^{z_3}\overline{E}_{\mathrm{e}}\overline{\lambda}_{\mathrm{e}}\,\Delta T\,\mathrm{d}z\right)\\+(d'_{11}+d'_{12})\left(\int_{z_0}^{z_1}\overline{E}_{\mathrm{f}}\overline{\lambda}_{\mathrm{f}}\,\Delta Tz\,\mathrm{d}z+\int_{z_1}^{z_2}\overline{E}_{\mathrm{d}}\overline{\lambda}_{\mathrm{d}}\,\Delta Tz\,\mathrm{d}z+\int_{z_2}^{z_3}\overline{E}_{\mathrm{e}}\overline{\lambda}_{\mathrm{e}}\,\Delta Tz\,\mathrm{d}z\right)\end{array}\right]-\lambda_{\mathrm{e}}\,\Delta T\end{array}\right\}$$

$z_2\leqslant z<z_3$ epidermis layer. (46)

(4) *For four-layer model (Stratum corneum, living epidermis, dermis and fat):*

$$\sigma_{xx}=(1+v_{\mathrm{f}})\overline{E}_{\mathrm{f}}\left\{\begin{array}{l}\left[\begin{array}{l}(a'_{11}+a'_{12})\left(\int_{z_0}^{z_1}\overline{E}_{\mathrm{f}}\overline{\lambda}_{\mathrm{f}}\,\Delta T\,\mathrm{d}z+\int_{z_1}^{z_2}\overline{E}_{\mathrm{d}}\overline{\lambda}_{\mathrm{d}}\,\Delta T\,\mathrm{d}z+\int_{z_2}^{z_3}\overline{E}_{\mathrm{e}}\overline{\lambda}_{\mathrm{e}}\,\Delta T\,\mathrm{d}z+\int_{z_3}^{z_4}\overline{E}_{\mathrm{sc}}\overline{\lambda}_{\mathrm{sc}}\,\Delta T\,\mathrm{d}z\right)\\+(b'_{11}+b'_{12})\left(\int_{z_0}^{z_1}\overline{E}_{\mathrm{f}}\overline{\lambda}_{\mathrm{f}}\,\Delta Tz\,\mathrm{d}z+\int_{z_1}^{z_2}\overline{E}_{\mathrm{d}}\overline{\lambda}_{\mathrm{d}}\,\Delta Tz\,\mathrm{d}z+\int_{z_2}^{z_3}\overline{E}_{\mathrm{e}}\overline{\lambda}_{\mathrm{e}}\,\Delta Tz\,\mathrm{d}z+\int_{z_3}^{z_4}\overline{E}_{\mathrm{sc}}\overline{\lambda}_{\mathrm{sc}}\,\Delta Tz\,\mathrm{d}z\right)\end{array}\right]\\+z\left[\begin{array}{l}(b'_{11}+b'_{12})\left(\int_{z_0}^{z_1}\overline{E}_{\mathrm{f}}\overline{\lambda}_{\mathrm{f}}\,\Delta T\,\mathrm{d}z+\int_{z_1}^{z_2}\overline{E}_{\mathrm{d}}\overline{\lambda}_{\mathrm{d}}\,\Delta T\,\mathrm{d}z+\int_{z_2}^{z_3}\overline{E}_{\mathrm{e}}\overline{\lambda}_{\mathrm{e}}\,\Delta T\,\mathrm{d}z+\int_{z_3}^{z_4}\overline{E}_{\mathrm{sc}}\overline{\lambda}_{\mathrm{sc}}\,\Delta T\,\mathrm{d}z\right)\\+(d'_{11}+d'_{12})\left(\int_{z_0}^{z_1}\overline{E}_{\mathrm{f}}\overline{\lambda}_{\mathrm{f}}\,\Delta Tz\,\mathrm{d}z+\int_{z_1}^{z_2}\overline{E}_{\mathrm{d}}\overline{\lambda}_{\mathrm{d}}\,\Delta Tz\,\mathrm{d}z+\int_{z_2}^{z_3}\overline{E}_{\mathrm{e}}\overline{\lambda}_{\mathrm{e}}\,\Delta Tz\,\mathrm{d}z+\int_{z_3}^{z_4}\overline{E}_{\mathrm{sc}}\overline{\lambda}_{\mathrm{sc}}\,\Delta Tz\,\mathrm{d}z\right)\end{array}\right]\\-\lambda_{\mathrm{f}}\,\Delta T\end{array}\right\}$$

$z_0\leqslant z<z_1$ fat layer, (47)

$$\sigma_{xx} = (1+v_{\mathrm{d}})\overline{E}_{\mathrm{d}} \left\{ \begin{array}{l} \left[\begin{array}{l} (a'_{11}+a'_{12})\left(\int_{z_0}^{z_1} \overline{E}_{\mathrm{f}}\overline{\lambda}_{\mathrm{f}}\,\Delta T\,\mathrm{d}z + \int_{z_1}^{z_2} \overline{E}_{\mathrm{d}}\overline{\lambda}_{\mathrm{d}}\,\Delta T\,\mathrm{d}z + \int_{z_2}^{z_3} \overline{E}_{\mathrm{e}}\overline{\lambda}_{\mathrm{e}}\,\Delta T\,\mathrm{d}z + \int_{z_3}^{z_4} \overline{E}_{\mathrm{sc}}\overline{\lambda}_{\mathrm{sc}}\,\Delta T\,\mathrm{d}z\right) \\ +(b'_{11}+b'_{12})\left(\int_{z_0}^{z_1} \overline{E}_{\mathrm{f}}\overline{\lambda}_{\mathrm{f}}\,\Delta T z\,\mathrm{d}z + \int_{z_1}^{z_2} \overline{E}_{\mathrm{d}}\overline{\lambda}_{\mathrm{d}}\,\Delta T z\,\mathrm{d}z + \int_{z_2}^{z_3} \overline{E}_{\mathrm{e}}\overline{\lambda}_{\mathrm{e}}\,\Delta T z\,\mathrm{d}z + \int_{z_3}^{z_4} \overline{E}_{\mathrm{sc}}\overline{\lambda}_{\mathrm{sc}}\,\Delta T z\,\mathrm{d}z\right) \end{array} \right] \\ +z\left[\begin{array}{l} (b'_{11}+b'_{12})\left(\int_{z_0}^{z_1} \overline{E}_{\mathrm{f}}\overline{\lambda}_{\mathrm{f}}\,\Delta T\,\mathrm{d}z + \int_{z_1}^{z_2} \overline{E}_{\mathrm{d}}\overline{\lambda}_{\mathrm{d}}\,\Delta T\,\mathrm{d}z + \int_{z_2}^{z_3} \overline{E}_{\mathrm{e}}\overline{\lambda}_{\mathrm{e}}\,\Delta T\,\mathrm{d}z + \int_{z_3}^{z_4} \overline{E}_{\mathrm{sc}}\overline{\lambda}_{\mathrm{sc}}\,\Delta T\,\mathrm{d}z\right) \\ +(d'_{11}+d'_{12})\left(\int_{z_0}^{z_1} \overline{E}_{\mathrm{f}}\overline{\lambda}_{\mathrm{f}}\,\Delta T z\,\mathrm{d}z + \int_{z_1}^{z_2} \overline{E}_{\mathrm{d}}\overline{\lambda}_{\mathrm{d}}\,\Delta T z\,\mathrm{d}z + \int_{z_2}^{z_3} \overline{E}_{\mathrm{e}}\overline{\lambda}_{\mathrm{e}}\,\Delta T z\,\mathrm{d}z + \int_{z_3}^{z_4} \overline{E}_{\mathrm{sc}}\overline{\lambda}_{\mathrm{sc}}\,\Delta T z\,\mathrm{d}z\right) \end{array} \right] \\ -\lambda_{\mathrm{d}}\,\Delta T \end{array} \right\}$$

$z_1 \leqslant z < z_2$ dermis layer, (48)

$$\sigma_{xx} = (1+v_{\mathrm{e}})\overline{E}_{\mathrm{e}} \left\{ \begin{array}{l} \left[\begin{array}{l} (a'_{11}+a'_{12})\left(\int_{z_0}^{z_1} \overline{E}_{\mathrm{f}}\overline{\lambda}_{\mathrm{f}}\,\Delta T\,\mathrm{d}z + \int_{z_1}^{z_2} \overline{E}_{\mathrm{d}}\overline{\lambda}_{\mathrm{d}}\,\Delta T\,\mathrm{d}z + \int_{z_2}^{z_3} \overline{E}_{\mathrm{e}}\overline{\lambda}_{\mathrm{e}}\,\Delta T\,\mathrm{d}z + \int_{z_3}^{z_4} \overline{E}_{\mathrm{sc}}\overline{\lambda}_{\mathrm{sc}}\,\Delta T\,\mathrm{d}z\right) \\ +(b'_{11}+b'_{12})\left(\int_{z_0}^{z_1} \overline{E}_{\mathrm{f}}\overline{\lambda}_{\mathrm{f}}\,\Delta T z\,\mathrm{d}z + \int_{z_1}^{z_2} \overline{E}_{\mathrm{d}}\overline{\lambda}_{\mathrm{d}}\,\Delta T z\,\mathrm{d}z + \int_{z_2}^{z_3} \overline{E}_{\mathrm{e}}\overline{\lambda}_{\mathrm{e}}\,\Delta T z\,\mathrm{d}z + \int_{z_3}^{z_4} \overline{E}_{\mathrm{sc}}\overline{\lambda}_{\mathrm{sc}}\,\Delta T z\,\mathrm{d}z\right) \end{array} \right] \\ +z\left[\begin{array}{l} (b'_{11}+b'_{12})\left(\int_{z_0}^{z_1} \overline{E}_{\mathrm{f}}\overline{\lambda}_{\mathrm{f}}\,\Delta T\,\mathrm{d}z + \int_{z_1}^{z_2} \overline{E}_{\mathrm{d}}\overline{\lambda}_{\mathrm{d}}\,\Delta T\,\mathrm{d}z + \int_{z_2}^{z_3} \overline{E}_{\mathrm{e}}\overline{\lambda}_{\mathrm{e}}\,\Delta T\,\mathrm{d}z + \int_{z_3}^{z_4} \overline{E}_{\mathrm{sc}}\overline{\lambda}_{\mathrm{sc}}\,\Delta T\,\mathrm{d}z\right) \\ +(d'_{11}+d'_{12})\left(\int_{z_0}^{z_1} \overline{E}_{\mathrm{f}}\overline{\lambda}_{\mathrm{f}}\,\Delta T z\,\mathrm{d}z + \int_{z_1}^{z_2} \overline{E}_{\mathrm{d}}\overline{\lambda}_{\mathrm{d}}\,\Delta T z\,\mathrm{d}z + \int_{z_2}^{z_3} \overline{E}_{\mathrm{e}}\overline{\lambda}_{\mathrm{e}}\,\Delta T z\,\mathrm{d}z + \int_{z_3}^{z_4} \overline{E}_{\mathrm{sc}}\overline{\lambda}_{\mathrm{sc}}\,\Delta T z\,\mathrm{d}z\right) \end{array} \right] \\ -\lambda_{\mathrm{e}}\,\Delta T \end{array} \right\}$$

$z_2 \leqslant z < z_3$ epidermis layer. (49)

$$\sigma_{xx} = (1+v_{\mathrm{sc}})\overline{E}_{\mathrm{sc}} \left\{ \begin{array}{l} \left[\begin{array}{l} (a'_{11}+a'_{12})\left(\int_{z_0}^{z_1} \overline{E}_{\mathrm{f}}\overline{\lambda}_{\mathrm{f}}\,\Delta T\,\mathrm{d}z + \int_{z_1}^{z_2} \overline{E}_{\mathrm{d}}\overline{\lambda}_{\mathrm{d}}\,\Delta T\,\mathrm{d}z + \int_{z_2}^{z_3} \overline{E}_{\mathrm{e}}\overline{\lambda}_{\mathrm{e}}\,\Delta T\,\mathrm{d}z + \int_{z_3}^{z_4} \overline{E}_{\mathrm{sc}}\overline{\lambda}_{\mathrm{sc}}\,\Delta T\,\mathrm{d}z\right) \\ +(b'_{11}+b'_{12})\left(\int_{z_0}^{z_1} \overline{E}_{\mathrm{f}}\overline{\lambda}_{\mathrm{f}}\,\Delta T z\,\mathrm{d}z + \int_{z_1}^{z_2} \overline{E}_{\mathrm{d}}\overline{\lambda}_{\mathrm{d}}\,\Delta T z\,\mathrm{d}z + \int_{z_2}^{z_3} \overline{E}_{\mathrm{e}}\overline{\lambda}_{\mathrm{e}}\,\Delta T z\,\mathrm{d}z + \int_{z_3}^{z_4} \overline{E}_{\mathrm{sc}}\overline{\lambda}_{\mathrm{sc}}\,\Delta T z\,\mathrm{d}z\right) \end{array} \right] \\ +z\left[\begin{array}{l} (b'_{11}+b'_{12})\left(\int_{z_0}^{z_1} \overline{E}_{\mathrm{f}}\overline{\lambda}_{\mathrm{f}}\,\Delta T\,\mathrm{d}z + \int_{z_1}^{z_2} \overline{E}_{\mathrm{d}}\overline{\lambda}_{\mathrm{d}}\,\Delta T\,\mathrm{d}z + \int_{z_2}^{z_3} \overline{E}_{\mathrm{e}}\overline{\lambda}_{\mathrm{e}}\,\Delta T\,\mathrm{d}z + \int_{z_3}^{z_4} \overline{E}_{\mathrm{sc}}\overline{\lambda}_{\mathrm{sc}}\,\Delta T\,\mathrm{d}z\right) \\ +(d'_{11}+d'_{12})\left(\int_{z_0}^{z_1} \overline{E}_{\mathrm{f}}\overline{\lambda}_{\mathrm{f}}\,\Delta T z\,\mathrm{d}z + \int_{z_1}^{z_2} \overline{E}_{\mathrm{d}}\overline{\lambda}_{\mathrm{d}}\,\Delta T z\,\mathrm{d}z + \int_{z_2}^{z_3} \overline{E}_{\mathrm{e}}\overline{\lambda}_{\mathrm{e}}\,\Delta T z\,\mathrm{d}z + \int_{z_3}^{z_4} \overline{E}_{\mathrm{sc}}\overline{\lambda}_{\mathrm{sc}}\,\Delta T z\,\mathrm{d}z\right) \end{array} \right] \\ -\lambda_{\mathrm{sc}}\,\Delta T \end{array} \right\}$$

$z_3 \leqslant z < z_4$ stratum corneum layer (50)

3. Results: case study

3.1. Thermal stress for one-layer model

Using the temperature profile solutions obtained in Section 2.1, the closed-form solutions of thermal stress can be obtained. For illustration, the temperature distribution obtained with the one-layer model for six different kinds of boundary conditions and uniform initial temperature is used to calculate the reluctant thermal stress in the skin tissue, as given below.

Case 1:

$$\begin{cases} T = T_\infty, & z = -H/2, \\ T = T_c, & z = H/2, \end{cases}$$

$$\sigma = \overline{E\lambda}\frac{2\alpha}{H}(T_\infty - T_0)\sum_{m=1}^{\infty}\left\{\frac{\beta_m}{\alpha\beta_m^2 + \dfrac{\varpi_b\rho_b c_b}{\rho c}}(1 - e^{-\alpha\beta_m^2 t-(\varpi_b\rho_b c_b/\rho c)t})\right.$$
$$\left.\times\left(\begin{array}{l}\dfrac{12z\sin(\beta_m H) - \dfrac{H}{2}\beta_m - \dfrac{H}{2}\beta_m\cos(\beta_m H)}{H^3}\beta_m^2 \\ +\dfrac{1-\cos(\beta_m H)}{\beta_m H} - \sin[\beta_m(z + H/2)]\end{array}\right)\right\}, \tag{51}$$

where $\beta_m = m/H\pi$, $m = 1, 2, 3, \ldots$.

Case 2:

$$\begin{cases} \partial T/\partial z = f_2, & z = -H/2, \\ T = T_c, & z = H/2, \end{cases}$$

$$\sigma = \overline{E\lambda} f_2 \frac{\alpha}{k}\frac{2}{H}\sum_{m=1}^{\infty}\left\{\frac{1}{\alpha\beta_m^2 + \dfrac{\varpi_b\rho_b c_b}{\rho c}}(1 - e^{-\alpha\beta_m^2 t-(\varpi_b\rho_b c_b/\rho c)t})\right.$$
$$\left.\times\left(\frac{12z}{H^3}\frac{H}{2}\beta_m\sin(\beta_m H) + \cos(\beta_m H) - 1}{\beta_m^2} + \frac{\sin(\beta_m H)}{\beta_m H} - \cos[\beta_m(z + H/2)]\right)\right\}, \tag{52}$$

where $\beta_m = (2m-1)/2H\pi$, $m = 1, 2, 3, \ldots$.

Case 3:

$$\begin{cases} -k\partial T/\partial z = h_3(f_3 - T), & z = -H/2, \\ T = T_c, & z = H/2, \end{cases}$$

$$\sigma = \overline{E\lambda}\frac{\alpha h_3(f_3 - T_0)}{k}\sum_{m=1}^{\infty}\left\{\frac{2[\beta_m^2 + (h_3/k)^2]}{H[\beta_m^2 + (h_3/k)^2] + h_3/k}\sin(\beta_m H)\right.$$
$$\left.\times\frac{(1 - e^{-\alpha\beta_m^2 t-(\varpi_b\rho_b c_b/\rho c)t})}{\alpha\beta_m^2 + \dfrac{\varpi_b\rho_b c_b}{\rho c}}\left(\begin{array}{l}\dfrac{12z\dfrac{H}{2}\beta_m + \dfrac{H}{2}\beta_m\cos(\beta_m H) - \sin(\beta_m H)}{H^3}\beta_m^2 \\ +\dfrac{1-\cos(\beta_m H)}{\beta_m H} - \sin[\beta_m(H/2 - z)]\end{array}\right)\right\}, \tag{53}$$

where β_m is the positive roots of $\beta_m\cot(\beta_m H) = -h_3/k$, $m = 1, 2, 3, \ldots$.

Case 4:

$$\begin{cases} T = T_\infty, & z = -H/2 \\ \partial T/\partial z = 0, & H/2, \end{cases}$$

$$\sigma = \overline{E}\overline{\lambda}\frac{2\alpha}{H}(T_\infty - T_0)\sum_{m=1}^{\infty}\left\{\frac{\beta_m}{\alpha\beta_m^2 + \dfrac{\varpi_b\rho_b c_b}{\rho c}}(1 - e^{-\alpha\beta_m^2 t - (\varpi_b\rho_b c_b/\rho c)t})\right.$$
$$\left.\times\left(\frac{12z\sin(\beta_m H) - \dfrac{H}{2}\beta_m - \dfrac{H}{2}\beta_m\cos(\beta_m H)}{H^3}\dfrac{}{\beta_m^2} + \frac{1 - \cos(\beta_m H)}{\beta_m H} - \sin[\beta_m(z + H/2)]\right)\right\}, \tag{54}$$

where $\beta_m = (2m-1)/(2H)\pi$, $m = 1, 2, 3, \ldots$.

Case 5:

$$\begin{cases} \partial T/\partial z = f_5, & z = -H/2, \\ \partial T/\partial z = 0, & z = H/2, \end{cases}$$

$$\sigma = \overline{E}\overline{\lambda}f_1\frac{\alpha}{k}\frac{2}{H}\sum_{m=2}^{\infty}\left\{\frac{1}{\alpha\beta_m^2 + \dfrac{\varpi_b\rho_b c_b}{\rho c}}(1 - e^{-\alpha\beta_m^2 t - (\varpi_b\rho_b c_b/\rho c)t})\right.$$
$$\left.\times\left(\frac{12z}{H^3}\frac{\dfrac{H}{2}\beta_m\sin(\beta_m H) + \cos(\beta_m H) - 1}{\beta_m^2} + \frac{\sin(\beta_m H)}{\beta_m H} - \cos[\beta_m(z + H/2)]\right)\right\}, \tag{55}$$

where $\beta_m = (m-1)/H\pi$, $m = 2, 3, 4, \ldots$.

Case 6:

$$\begin{cases} -k\partial T/\partial z = h_6(f_6 - T), & z = -H/2, \\ \partial T/\partial z = 0, & z = H/2, \end{cases}$$

$$\sigma = \overline{E}\overline{\lambda}\frac{\alpha h_6(f_6 - T_0)}{k}\sum_{m=1}^{\infty}\left\{\frac{2[\beta_m^2 + (h_6/k)^2]}{H[\beta_m^2 + (h_6/k)^2] + h_6/k}\cos(\beta_m H)\frac{(1 - e^{-\alpha\beta_m^2 t - (-\varpi_b\rho_b c_b/\rho c)t})}{\alpha\beta_m^2 + \dfrac{\varpi_b\rho_b c_b}{\rho c}}\right.$$
$$\left.\times\left(\frac{12z}{H^3}\frac{1 - \cos(\beta_m H) - \dfrac{H}{2}\beta_m\sin(\beta_m H)}{\beta_m^2} + \frac{\sin(\beta_m H)}{\beta_m H} - \cos[\beta_m(z - H/2)]\right)\right\} \tag{56}$$

where β_m is the positive roots of $\beta_m\tan(\beta_m H) = h_6/k$, $m = 1, 2, 3, \ldots$.

The above closed-form solution for single-layer model, although much simplified, provides an essential calibration tool for more complex numerical analysis. For more complicated cases, the complex structure of skin tissue limits the accessibility needed for a detailed experimental investigation and theoretical solution of the thermomechanical behavior. This reason has motivated the use of numerical simulation to understand the thermomechanics of skin tissue. As case studies, the temperature and corresponding stress fields obtained with the one-layer skin model for three different thermal boundary conditions (Table 1) are plotted in Fig. 7(a) and (b).

Table 1
Parameter used in one-dimensional analytical model

Case 1: $\begin{cases} T = T_\infty, \ z = -H/2 \\ T = T_c, \ z = H/2 \end{cases}$	$T_\infty = 90\,^\circ\mathrm{C}$, $T_c = 37\,^\circ\mathrm{C}$
Case 2: $\begin{cases} -k\partial T/\partial z = f_2, \ z = -H/2 \\ T = T_c, z = H/2 \end{cases}$	$f_2 = 2500\,\mathrm{W/m^2}$ $T_c = 37\,^\circ\mathrm{C}$
Case 3: $\begin{matrix} -k\partial T/\partial z = h_f(T_f - T), \ z = -H/2 \\ T = T_c, z = H/2 \end{matrix}$	$T_f = 90\,^\circ\mathrm{C}, h_f = 2500\,\mathrm{W/m^2\,^\circ C}$ $T_c = 37\,^\circ\mathrm{C}$
Young's modulus of skin, E	0.6 MPa
Poisson ratio	0.48
Thermal expansion coefficient of skin	0.0001/K

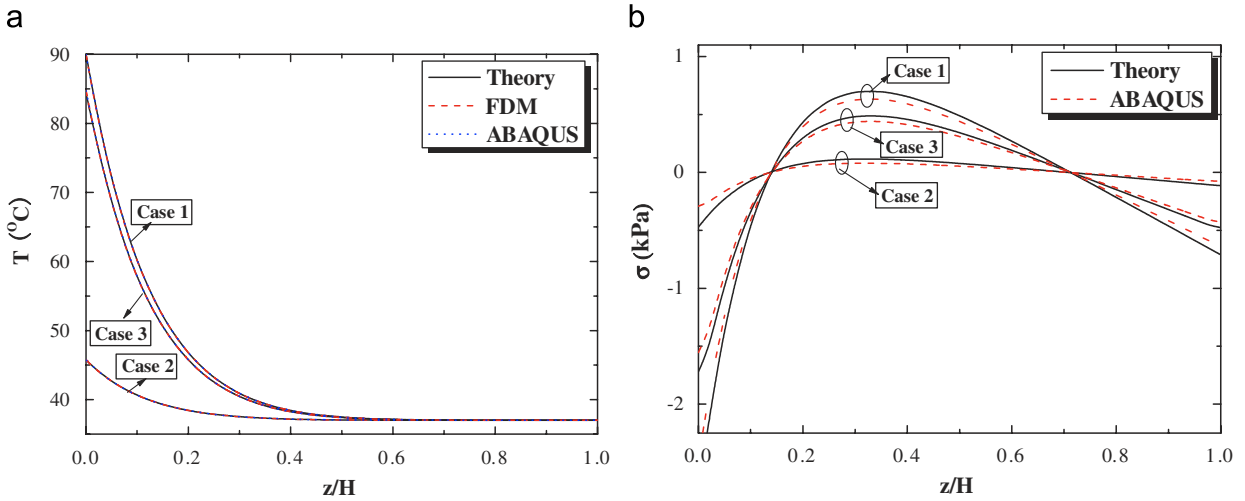

Fig. 7.

These can be used to check the accuracy of predictions using numerical tools such as the FEM, which is used later in this study, for the structure of skin which is very complicated and cannot normally be treated as a single homogeneous layer. Note that, for the one-layer model, the results of Fig. 7 demonstrate excellent agreement between analytical and numerical predictions. More details of the numerical approach are described in the following sections; for FEM, the commercially available code ABAQUS™ is used.

3.2. Thermomechanical analysis with 1-D skin model

(1) *Description of the problem*: The skin is initially kept at constant temperature. At $t = 0$, the skin surface initially at normal temperature is suddenly taken into contact with a hot source of constant temperature 90 °C; after contacting for 15 s, the hot source is removed and the skin is cooled by natural convection of environmental air ($T_e = 25\,^\circ\mathrm{C}$, $h = 7\,\mathrm{W/m^2\,K}$) for 30 s. The temperature fields are obtained by using the FDM, which are subsequently used to calculate the corresponding thermal stress field.

Treatment of skin: For the heat transfer process, the skin is divided into three layers with different properties: epidermis with thickness of 0.1 mm, dermis with thickness of 1.5 mm and subcutaneous fat with thickness of 4.4 mm. Blood perfusion is only considered in the dermis layer while metabolic heat generation is considered in all three layers. The relevant parameters used for both heat transfer and thermal stress analyses

Table 2
Parameters for one-dimensional numerical heat transfer analysis

	Epidermis	Dermis	Subcutaneous fat
Thickness (mm)	0.1	1.5	4.4
Density × specific heat ($\times 10^6$ J/m^3 K)	3.182	2.846	1.975
Thermal conductivity (J/mk)	0.21	0.37	0.16
Blood perfusion rate (ml Blood/ml tissue/s)	0	0–0.1	0
Metabolic heat generation rate (W/m^3)	368.1	368.1	368.3

Table 3
Parameters for one-dimensional numerical thermal stress analysis

Layers of skin		Thermal expansion coefficient	Poisson ratio	Young's modulus (MPa)		
				One-layer model	Three-layer model	Four-layer model
Epidermis	Stratum corneum	0.0001	0.48	0.6	100	2000
	Living epidermis	0.0001	0.48			100
Dermis		0.0001	0.48		10	10
Subcutaneous fat		0.0001	0.48		0.01	0.01

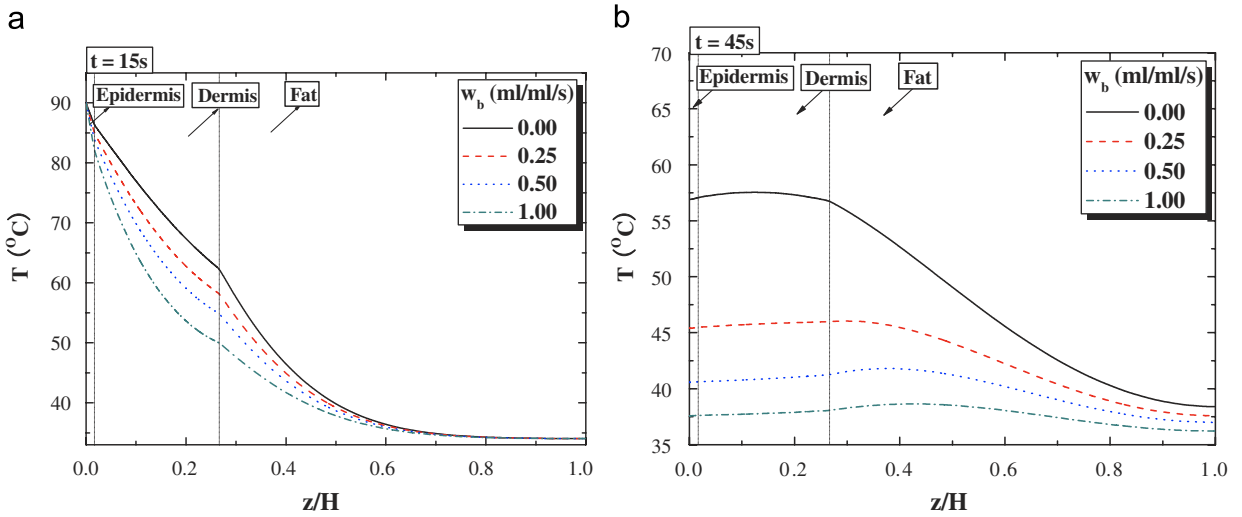

Fig. 8.

are summarized in Tables 2 and 3 (taken from Dahan et al., 2004; Delalleau et al., 2006; Duck, 1990; Elkins and Thomson, 1973; Hendriks et al., 2006; Henriques and Moritz, 1947; Roetzel and Xuan, 1998; Sejrsen, 1972; Torvi and Dale, 1994). It should be noted here, since there is no published data available in the literature, the thermal expansion coefficient is assumed to be $1 \times 10^{-4}/^{\circ}$C is this study, which is similar to those assumed by other researchers (L'Etang et al., 2006) and in the same order as the experimental measurement of other biological tissues (Xu et al., 2007).

Calculation of burn injury: The skin thermal damage is calculated by use of the burn integration of Eq. (26), with the frequency factor $A = 3.1 \times 10^{98}$ and the ratio of activation energy to universal gas constant $E_a/R = 75\,000$ (see Henriques, 1947). Note that it is now widely accepted that: $\Omega = 0.53$, first degree burn; $\Omega = 1.0$, second degree burn; $\Omega = 10^4$, third degree burn.

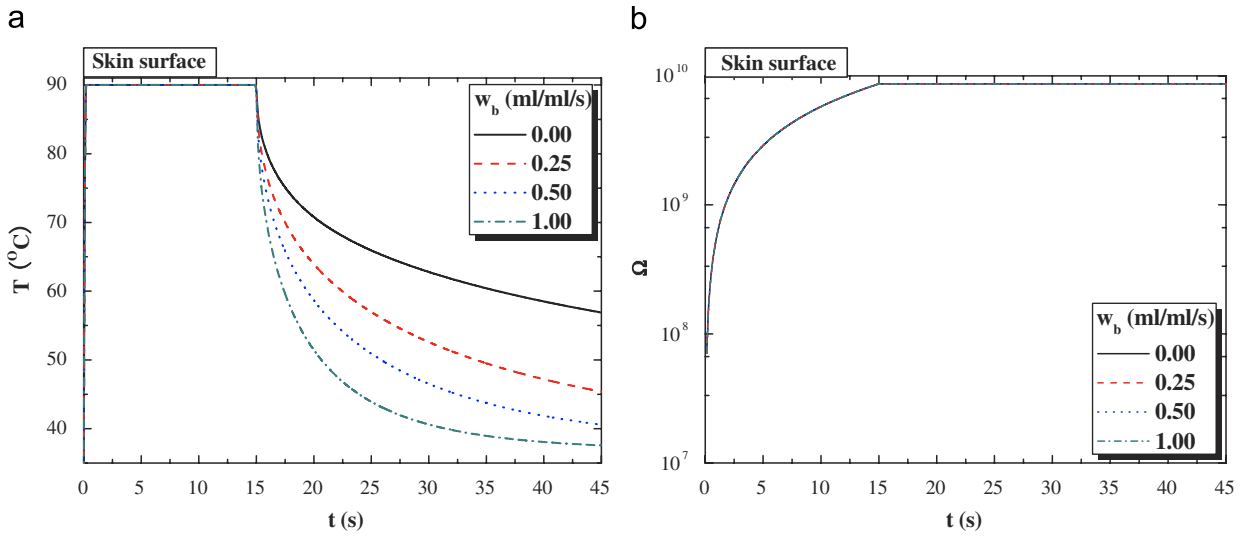

Fig. 9.

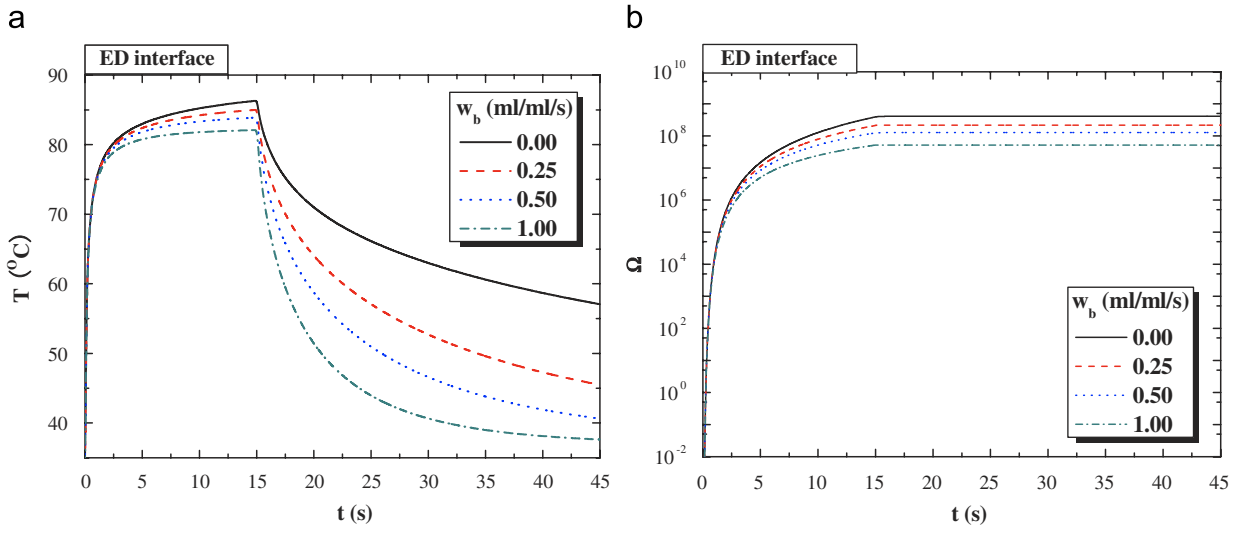

Fig. 10.

Results:

Influence of dermis blood perfusion: The temperature distribution in the skin at the end of heating, $t = 15$ s, and cooling, $t = 45$ s, is shown separately in Figs. 8(a) and (b) for selected blood perfusion rates, with the skin surface heat transfer coefficient fixed at $h = 7\,\mathrm{W/m^2\,K}$, which is natural convective cooling. Figs. 9 and 10 plot the corresponding levels of temperature and burn damage at the skin surface and epidermis–dermis interface (ED interface) as functions of time, respectively, whilst Figs. 11 and 12 present the temporal and spatial distributions of stress, respectively. Note that the effect of blood perfusion rate has a significantly larger influence on temperature distribution during cooling than that during heating. In general, the skin temperature decreases with increasing blood perfusion rate. As the skin surface is kept at 90 °C for 15 s during which the thermal injury is incurred, the blood perfusion rate has little effect on the burn damage on skin surface, Fig. 9(b), and has a weak influence on that at the ED interface, Fig. 10(b). Both the skin surface and ED interface are subjected to large tensile stresses, typically >10 MPa, Figs. 11 and 12, especially during

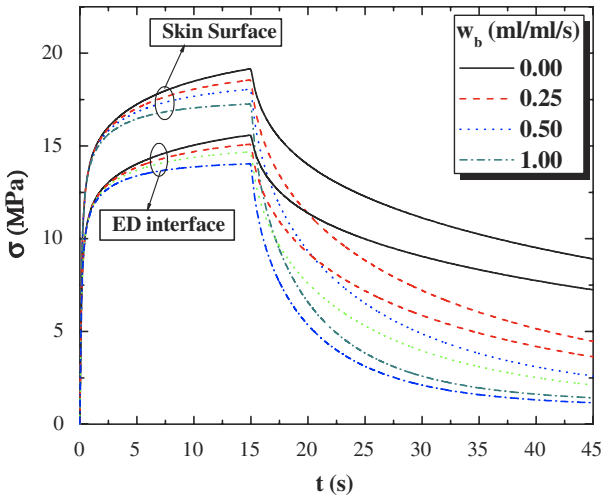

Fig. 11.

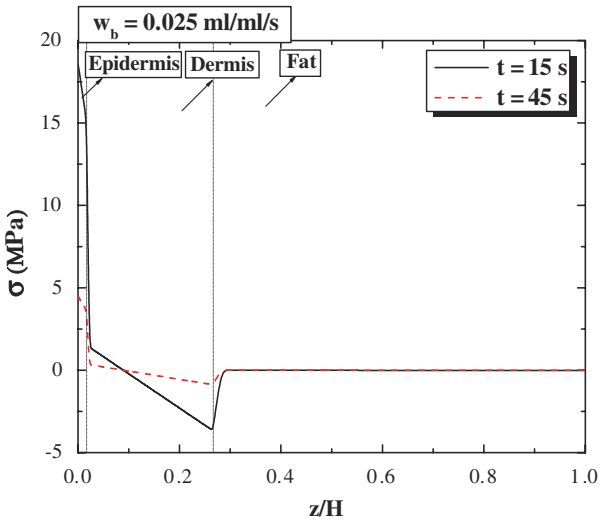

Fig. 12.

heating, indicating severe thermal damage, which is consistent with the results of Figs. 9(b) and 10(b). The large tensile stresses at skin surface and ED interface predicted by the multi-layer skin model are in sharp contrast with those obtained with the one-layer model, Fig. 7. Overall, the skin has endured severe damage, as evinced by absolute values of Ω being 4 orders of magnitude beyond the threshold for third degree burns. This is not unexpected given the boundary conditions.

Influence of cooling heat transfer coefficient: For selected values of surface heat transfer coefficient, h, and with the blood perfusion rate in the dermis fixed at $\varpi_b = 0.025\,\mathrm{ml\,Blood/ml\,tissue/s}$, Fig. 13 plots the temperature distribution at the end of cooling ($t = 45\,\mathrm{s}$). Note that, the results of Fig. 13 are similar to those shown in Fig. 8(b), suggesting that increasing the surface heat transfer coefficient, h, with blood perfusion rate, ϖ_b, being fixed has a similar effect as that by increasing ϖ_b with h being fixed. Correspondingly, the variations of temperature and damage integration distributions with time at the ED interface have similar trends as those exhibited in Fig. 10 and hence are omitted from display here.

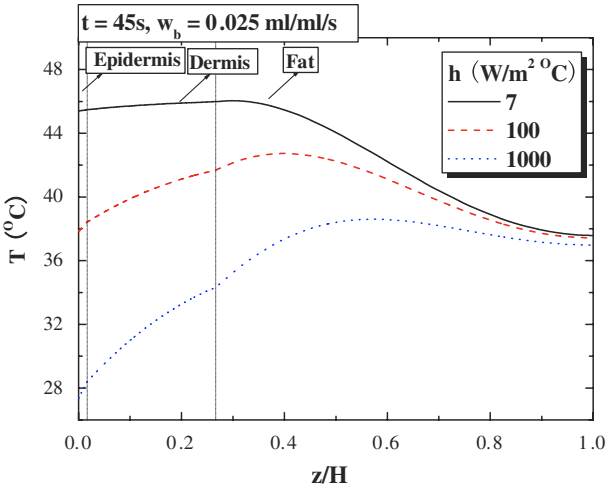

Fig. 13.

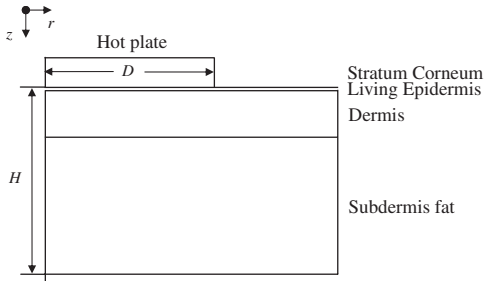

Fig. 14.

3.3. Thermomechanical analysis with two-dimensional skin model

(1) *Description of the problem*: The two-dimensional (2-D) physical model used to study the thermomechanical behavior of skin is presented in Fig. 14. A similar model has been used by Diller and Hayes (1983) and Ng and Chua (2000) to study the thermal damage of skin. Initially, the skin of thickness H and radius R_0 is at a steady state with the surface cooled by natural convection of environmental air ($h = 7\,\mathrm{W/m^2\,K}$). At time $t = 0$, the skin surface is suddenly in contact with a hot plate (90 °C) of radius D (assumed $D = H$) while the base of the skin is kept at constant temperature. The boundary at $r = R_0$ is a set isothermally as normal skin temperature. The skin is free to expand except at the base where it is fixed due to connection with the body core. The parameters used in the FEM simulation are given in Table 4; other parameters are identical to those used for 1-D analysis (Tables 2 and 3).

(2) *Results*:

Mesh and sensitivity analysis: The FE mesh of the 2-D skin model is shown in Fig. 15. Since stress singularity exists at the corner of contact, the mesh is refined in this region. The problem is solved by commercially available FEM package ABAQUS™. Sensitivity analysis is first performed to study the influence of different parameters: ratio of skin layer radius to thickness R_0/H, time step Δt and grid density N. According to the results (not shown here for brevity), in the following computation, these parameters are chosen as $R_0/H = 20$, $\Delta t = 0.1\,\mathrm{s}$ and $N = 19\,420$.

Verification of the model: Presently there is no experimental data or closed-form solution on stress field available to make a comparison, and hence only the temperature field is verified here. The calculated temperature distribution accounting for the influence of blood perfusion is compared in Fig. 16 with that

Table 4
Parameters used in two-dimensional skin model

	Stratum corneum	Living epidermis
Thickness (mm)	0.020	0.080
Density × specific heat ($\times 10^6$ J/m^3 K)	3.182	3.182
Thermal conductivity (J/mK)	0.21	0.21
Blood perfusion rate (ml Blood/ml tissue/s)	0	0
Thermal expansion coefficient	0.0001	0.0001
Poisson ratio	0.48	0.48
Young's modulus (MPa)	2000	100

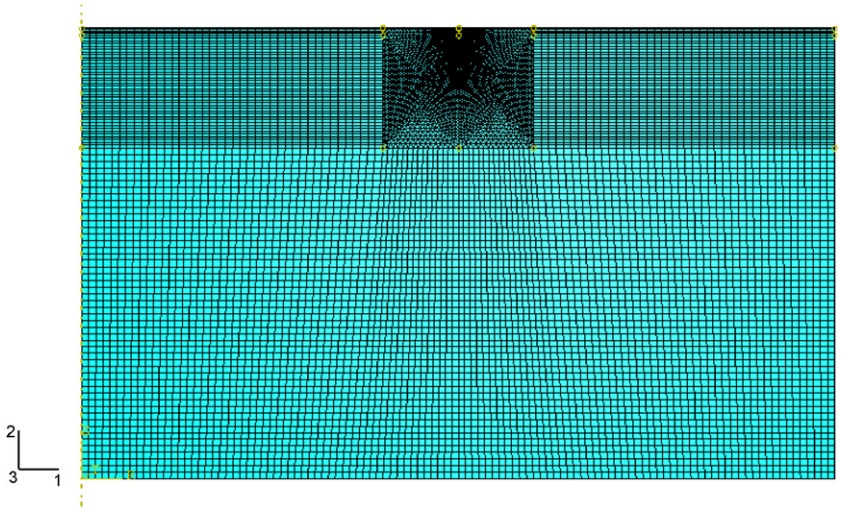

Fig. 15.

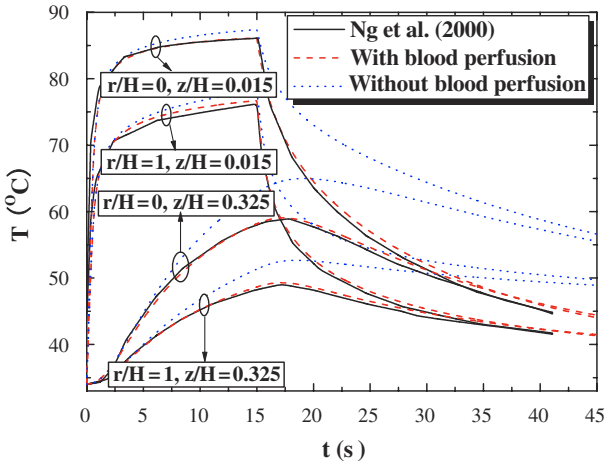

Fig. 16.

obtained by Ng and Chua (2000) for the same problem, where Ng and Chua applied a FE model to study a pure heat transfer problem in skin tissue. Good agreement is observed, demonstrating the feasibility of the present approach. Note that the temperature obtained without considering the influence of blood perfusion is significantly higher than that with this effect considered, which is also plotted.

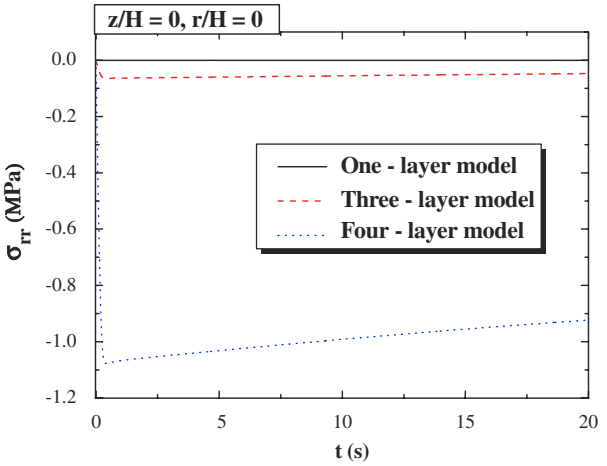

Fig. 17.

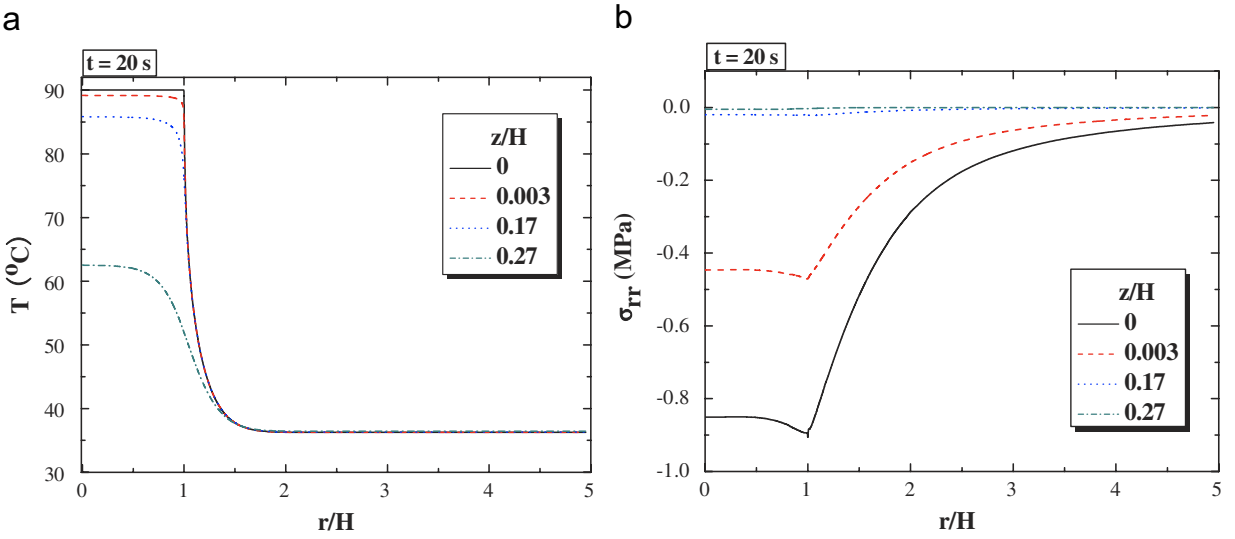

Fig. 18.

Influence of the number of layers in skin model: Although the stratum corneum layer has been shown to play an important role in the thermal and mechanical behaviors of skin, e.g. (Magnenat-Thalmann et al., 2002; Rigal and Leveque, 1985), its effect is often neglected in most studies due to its relatively small thickness. Here, in order to study its effect results predicted from three different axi-symmetrical skin models: (a) a one-layer model, where the skin is treated as a homogenous medium with constant properties; (b) a three-layer model, where the skin is consisted of epidermis, dermis and subcutaneous fat layers; (c) a four-layer model, where the skin is composed of stratum corneum, epidermis, dermis and subcutaneous fat layers. Relevant material and geometrical parameters used for each layer can be found in Tables 2–4. Note that the stratum corneum layer is very thin, about 0.02 mm in thickness (Table 4). Also, whilst blood perfusion occurs only in the dermis, Young's modulus varies by approximately an order of magnitude as each layer is crossed, being 2 GPa for the stratum corneum and 0.01 MPa for the subcutaneous fat layer. It is remarkable that this dramatic change in elastic modulus occurs over a distance less than 2 mm; see Table 2.

Fig. 17 plots the radial stress, σ_{rr}, at the center of skin surface ($r/H = 0, z/H = 0$) as a function of time obtained separately with the one-, three- and four-layer skin models. The results clearly show a very large

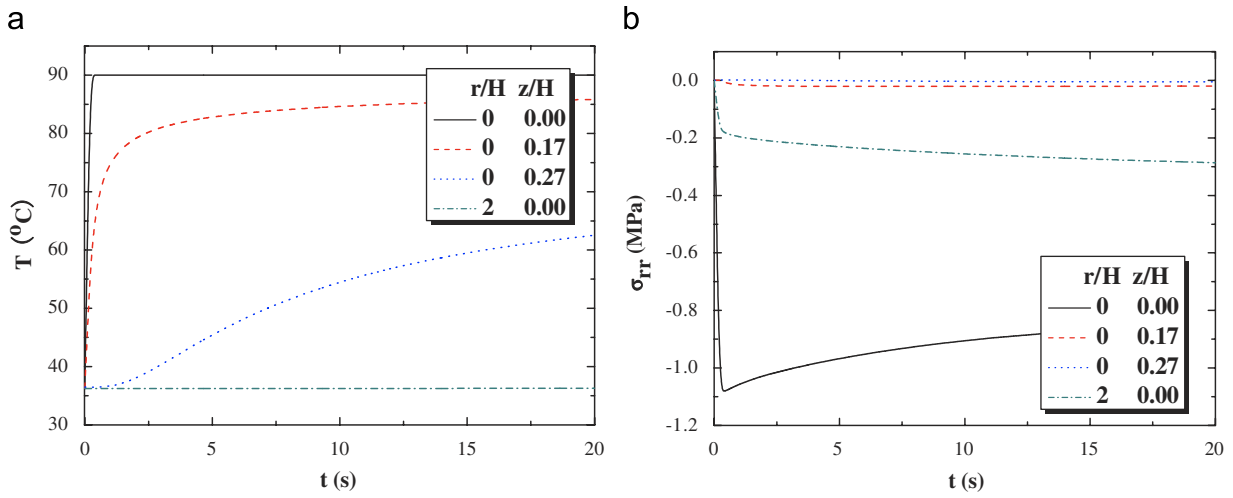

Fig. 19.

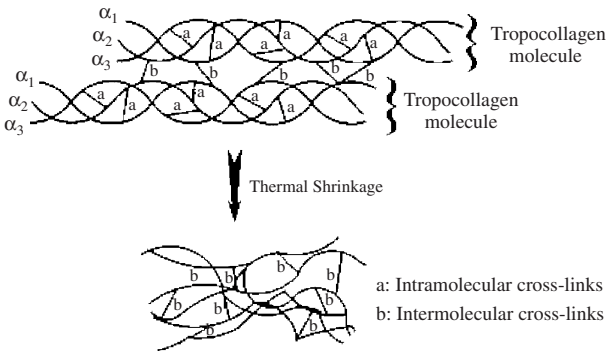

Fig. 20.

discrepancies between different models, highlighting the important role of stratum corneum layer in any thermomechanical modeling of skin. In particular, with the stratum corneum layer considered, a large compressive stress is developed on skin surface as a result of sudden heating (Fig. 17): this feature is not captured by the one- or three-layer skin model.

Spatial and temporal distributions of temperature and stress: Figs. 18(a) and (b) show the temperature and stress distributions at different skin depths at $t = 20$ s, whilst Figs. 19(a) and (b) show the variations of temperature and stress distributions with time at different skin locations. Note that, although the heat penetrates deep into the skin, the results of Figs. 18 and 19 show that the thermal injury and thermal stress are only limited to the top layers of the skin, in the stratum corneum and the epidermis. Fig. 19 for temperature and stress history shows a qualitatively distinct variation at different positions: the stress at skin surface ($r/H = 0$, $z/H = 0$) has the much larger variation than those at deeper depth ($z/H = 0.17$, $z/H = 0.27$) and that at far out of the heating region ($r/H = 2$, $z/H = 0$), which is due to the heating conduction process as can be seen from Fig. 19(a).

4. Discussion

4.1. Mechanisms of thermal denaturation of collagen

Skin biothermomechanics here is defined as the response of skin under thermomechanical loading, which leads to damage—the thermal denaturation of collagen. Collagen is the major dermal constituent and

accounts for approximately 60–80% of the dry weight of fat-free skin (Ebling et al., 1992; Reihsner et al., 1995) and 18–30% of the volume of dermis (Ebling et al., 1992). The collagen in human dermis is mainly the periodically banded, interstitial collagen (types I, III and IV), where about 80–90% is type I collagen and 8–12% is type III collagen. As noted, skin also contains a small mount of elastin but which is very thermally stable (Davidson et al., 1990), for example elastin can survive boiling for several hours with no apparent change, and does not need attention here.

Type I collagen has a domain within the triple helix that is completely devoid of hydroxyproline. Since hydroxyproline readily forms hydrogen bonds that stabilize the molecule, its absence makes this domain particularly susceptible to thermal damage (Miles and Bailey, 2001). There are two levels of organization where breakdown is thermodynamically significant (Young, 1998): one is the collagen molecule itself, in which three peptide chains are twisted around each other to form a helical, rod-shaped molecule; the other is the semi-crystalline fibril in which collagen molecules are assembled side-by-side in a staggered manner with the long axis of each molecule aligned with axial orientation of the fibril. When collagen is heated, the heat-labile intramolecular crosslinks are broken, as shown in Fig. 20, and the collagen undergoes a transition from a highly organized crystalline structure to a random, gel-like state, which is the denaturation process (Flory and Garrett, 1958). Collagen shrinkage occurs through the cumulative effect of the unwinding of the triple helix, due to the destruction of the heat-labile intramolecular cross-links, and the residual tension of the heat-stable intermolecular cross-links (Allain et al., 1980; Arnoczky and Aksan, 2000; Flory and Garrett, 1958).

The effects of heating on collagen can be reversible or irreversible and the precise heat-induced behavior of collagenous tissue and shrinkage depend on several factors, including the collagen content (Chvapil and Jensovsky, 1963), the maximum temperature reached and exposure time (Allain et al., 1980), the mechanical stress applied to the tissue during heating (Chen et al., 1998a), and aging (Chvapil and Jensovsky, 1963; Le Lous et al., 1985).

Different metrics have been used to characterize the thermal denaturation and heating-induced damage of collagen and collagenous tissues, including biological metrics such as enzyme deactivation (Bhowmick and Bischof, 1998) and extravasation of fluorescent-tagged plasma proteins (Green and Diller, 1978), thermal metrics such as changes in enthalpy (Jacques, 2006; Miles, 1993), mechanical metrics such as thermal shrinkage (Chen et al., 1998a, b, Kondo et al., 2005; Lin et al., 2006) and optical metrics such as thermally induced loss of birefringence (de Boer et al., 1998; Pearce et al., 1993; Srinivas et al., 2004; Thomsen, 1991). Although the shrinkage of collagen due to thermal denaturation have been widely used and suggested to be used as a convenient continuum metric of thermal damage (Diller and Pearce, 1999; Fung, 1990), Wells et al. (2004) point out that equilibrium shrinkage may not be a universal metric to measure thermal damage. Rather, there is a need to identify an independent metric by which one can determine the extent of thermal damage (Baek et al., 2005). Diller and Pearce (1999) point out that the dimensionless indicator of damage, Ω, is, in fact, the logarithm of the relative concentration of 'reactants', or un-denatured collagen, in the collagen denaturation process, where Ω can be alternatively considered as

$$\Omega(t) = \ln\left[\frac{C(0)}{C(t)}\right]. \tag{57}$$

$C(0)$ and $C(t)$ are the initial concentration and the concentration remaining at time t of un-denatured collagen. The degree of thermal denaturation, defined to be the fraction of denatured collagen, and denoted by $\mathrm{Deg}(t)$, can be calculated as

$$\mathrm{Deg}(t) = \frac{C(0) - C(t)}{C(0)} = 1 - \exp[-\Omega(t)]. \tag{58}$$

However, there are comparatively few studies of the thermal denaturation of skin tissue (Le Lous et al., 1982, 1985; McHugh et al., 1997; Melling et al., 2000; Pierce et al., 2004; Reihsner et al., 2000), despite skin dermis being mainly composed of collagen.

4.2. Property variations due to thermal denaturation of collagen

Denaturation of collagen occurs as the temperature of the tissue increases. As well as structural changes, the hydration level of collagen also changes, which may involve an initial liberation and subsequent absorption of

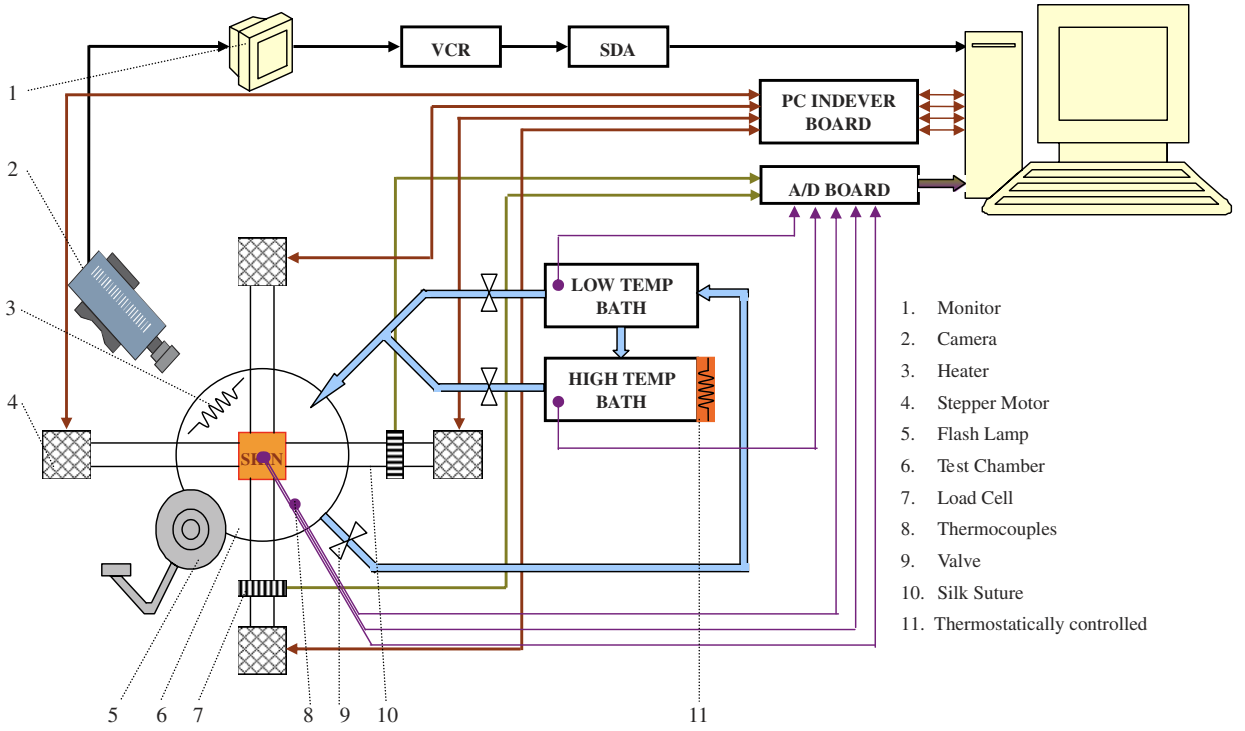

Fig. 21.

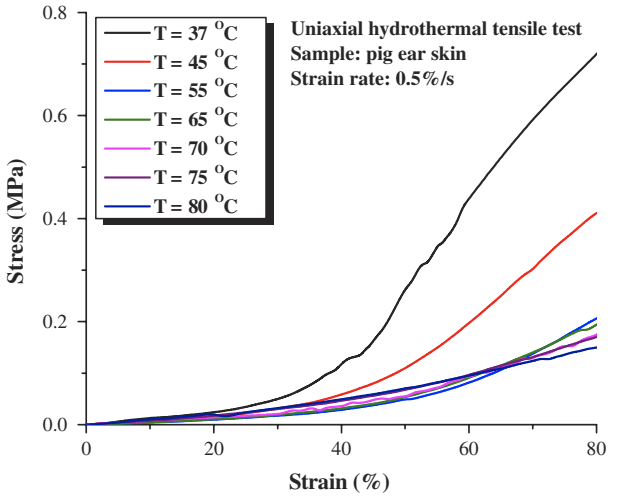

Fig. 22.

water (Humphrey, 2003). Not surprisingly, thermal denaturation of a collagenous tissue, can result in marked changes in the thermal (Davis et al., 2000), mechanical (Aksan and McGrath, 2003; Chae et al., 2003; Chao et al., 2001; Chen and Humphrey, 1998; Chen et al., 1997, 1998a, b; Diaz et al., 2001) and optical properties (Agah et al., 1996; Bosman, 1993; Jun et al., 2003; Lin et al., 1996). For example, increased extensibility of soft tissues due to thermal treatment has been observed in both uniaxial (Chachra et al., 1996; Chen and Humphrey, 1998; Lennox, 1949) and biaxial studies (Harris et al., 2003; Wells et al., 2004).

It should be pointed out that, in the analysis so far, it has been assumed that the thermal and mechanical properties of the skin layers are constant, i.e., independent of the thermal denaturation (shrinkage and

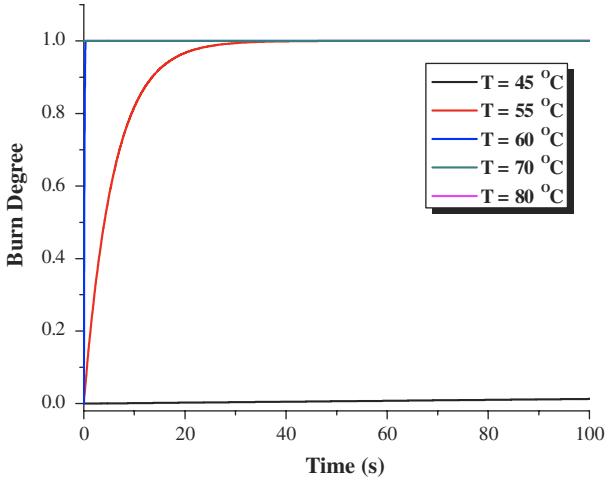

Fig. 23.

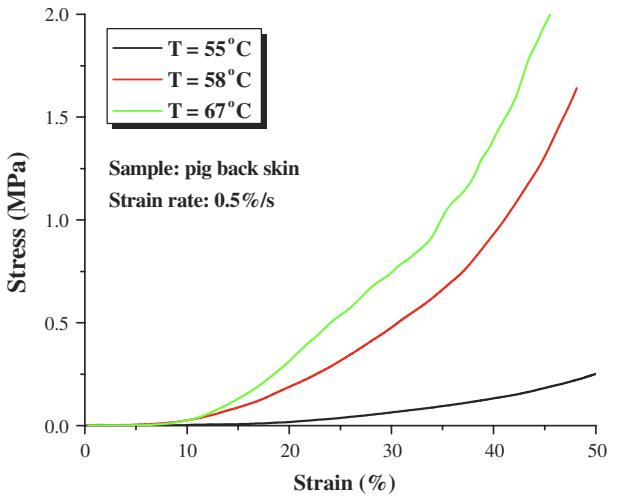

Fig. 24.

damage). Existing test data on the effects of temperature and damage on the physical properties of skin are scarce, and will be the subject of a future study. A schematic of the hydrothermal biaxial tensile testing system designed and fabricated by us is shown in Fig. 21. Biaxial mechanical test is chosen in the present system design for the following reasons: (1) *in vivo*, skin is loaded biaxially; (2) as the fibers in skin are multidirectional, the orientation of the fibers with respect to the load axis must be taken into account; (3) for incompressible or nearly incompressible materials biaxial mechanical testing can be used to obtain the material parameters for 3-D constitutive models; (4) pursuit of a multiaxial analysis is of clinical importance to surgeons for if the orientation of maximum extensibility is known, the excision can be planned to optimize wound closure.

Based on testing system of Fig. 21, preliminary results from uniaxial tensile tests on pig skin samples under different temperatures are given in Fig. 22. The results shown that the stress–strain curves are shifted downward as the temperature is increased, but little change is observed above 55 °C. The downward shift may be attributed to hydration change with temperature, whilst the little change above 55 °C can be explained by the thermal damage process, as shown in Fig. 23 in terms of thermal damage degree (Eq. (58)). When the temperature is raised above 55 °C, the collagen in the dermis is denaturized almost instantly, while at 45 °C, the process of denaturation is slow.

Similarly, a hydrothermal compressive loading system has been designed and fabricated to study the thermomechanical behavior of skin tissue under compression. The hydrothermal compressive tests of pig skin

samples under different temperatures have also been performed, with preliminary results shown in Fig. 24. Contrary to the tensile response of Fig. 22, the compressive stress–strain curve is shifted upward with the increase of temperature, even at temperatures above 55 °C. More experiments need to be carried out to understand this interesting phenomenon.

4.3. Thermal pain

The International Association for the Study of Pain defines pain as: 'an unpleasant sensory and emotional experience associated with actual or potential tissue damage, or described in terms of such damage'. Generally, pain can be classified as: (1) nociceptive pain where there is activation or sensitization of peripheral nociceptors; (2) inflammatory pain where damaged tissue, inflammatory and tumor cells release chemical mediators which activate or modify the stimulus response properties of nociceptor afferents; (3) neuropathic pain where there is injury or acquired abnormalities of peripheral or central neural structures.

As the first cells in the series of neurons leading to the sensation of nociceptive pain, nociceptors (special receptors for pain sensation) transduct mechanical, chemical and/or thermal energy to ionic current leading to action potentials: these potentials are conducted from the peripheral sensory site to the synapse in the central nervous system, and converted into neurotransmitter release at the presynaptic terminal (frequency modulation) (McCleskey and Gold, 1999).

It should be pointed out that whilst the mean mechanical threshold of nociceptors in the skin lies in the range of about 0–0.6 MPa and mainly between 0.1–0.2 MPa (James and Richard, 1996), our results presented in Section 3 (with the four-layer model) demonstrate that the thermal stress can be significantly larger than the threshold. This suggests that, in addition to heating, thermal stress may also contribute to thermal pain. Other supporting evidence shows that, for the same level of nociceptor activity, a heat stimulus evokes more pain than a mechanical stimulus and that tissue deformation due to heating and cooling may explain the origins of pain (Reuck and Knight, 1966; Van Hees and Gybels, 1981).

In a future study, a holistic model for quantifying thermal pain, which directly correlates the stimulus and pain sensation level, will be developed, by coupling the thermomechanical models developed in this study and the biophysical and neurological mechanisms of pain sensation.

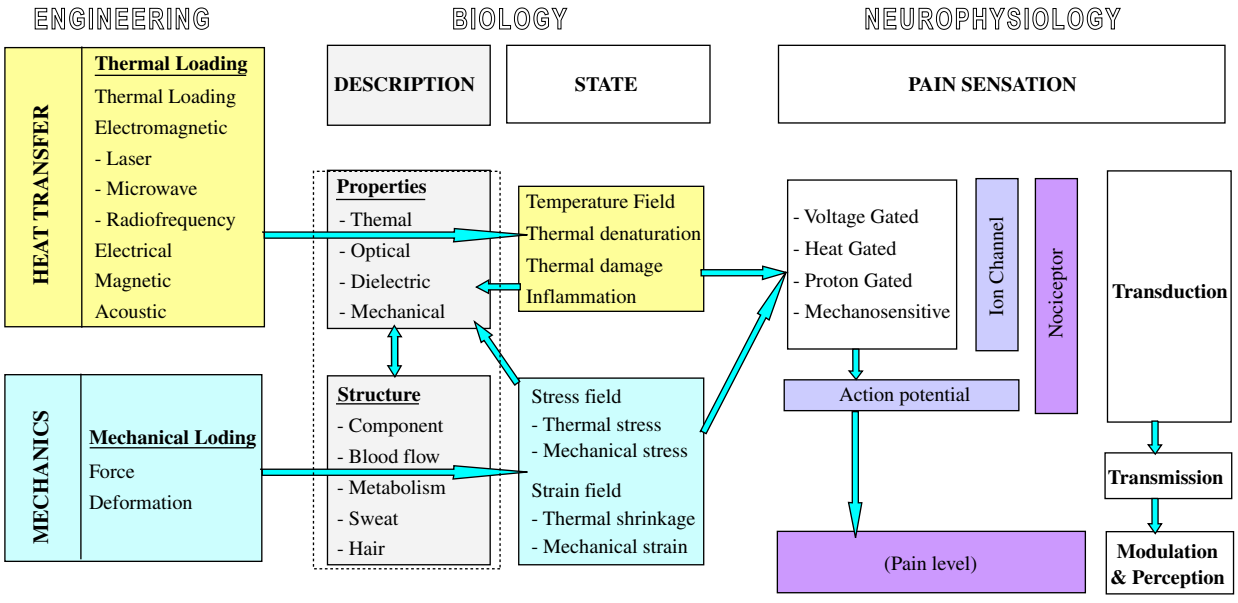

Fig. 25.

4.4. Roadmap of skin biothermomechanics and thermal pain

From above, we know that 'Skin Biothermomechanics and Thermal Pain' is a highly interdisciplinary area involving bioheat transfer, biomechanics and neurophysiology. The relationship between these areas is schematically shown in Fig. 25. The skin tissue is characterized by its *structure*, such as component, blood flow, metabolism etc., and *properties*, such as thermal, mechanical, optical and dielectric properties. When *thermal loading* (such as contact heating, electromagnetic energy or acoustic energy) and/or *mechanical loading* (such as force or deformation) are applied to skin tissue, according to the skin *description*, there will be corresponding skin *state*, such as temperature distribution, thermal damage/inflammation distribution and stress/strain distribution. The *state* will then decide the level of *pain sensation* with the help of the neural system.

A better understanding of skin tissue properties, skin bioheat transfer and kinetics of thermal damage, skin biomechanics and skin thermal pain sensation, all promise to contribute to the continuing refinement of skin thermomechanics and thermal pain.

5. Conclusions

For heat transfer, the skin is treated as a layered material, whose overall properties are assembled in a composite manner. For a simple, 1-D single layer case, closed-form solutions have been obtained for different conditions. For more complex cases, numerical methods have been used. Additionally, heat transfer models, which incorporate sweating effects and heat diffusion by hair above skin have also been developed.

A scheme is subsequently developed for calculating the layer-wise stresses induced inside skin tissue during a thermal loading. The skin is treated as a layered—'laminated'—material, whose overall properties are assembled in a composite manner, and its thermomechanical behavior is simplified to be a 'sequentially-coupled' problem. The formulation is based on the heat conduction equation and the solution of temperature profile, coupled to a thermo-elastic model derived from classical laminate theory. Initially, for the simplest case, the skin is regarded as a single-layer material, whose thermal response can be solved in closed form without computational assistance: although much simplified, this provides an essential calibration tool for more complex numerical analysis. For multi-layer skin model, even for a 1-D treatment of skin, an exact solution is difficult to get, so numerical methods (finite difference method and finite element method) are used to calculate the temperature, burn damage and thermal stress distributions in the skin tissue. Accordingly, the influences of different parameters on the thermomechanical response have been investigated, in order to assess their relative contributions, with the following interesting results.

The following conclusions are drawn:

- Blood perfusion has little influence on burn damage, but great influence on the temperature distribution in skin, which inversely influences the corresponding thermal stress greatly.
- A simple 1-D solution predicts very high stresses compared to an axi-symmetrical solution, but the latter stresses remain above the pain threshold in view of the high surface temperatures specified in these solutions.
- Although very thin, the influence of stratum corneum layer on thermal stress development in skin is significant and should not be neglected in any modeling effort.
- In addition to heating/cooling, skin thermal stresses may also contribute to thermal pain.

Other important issues, such as the variation of skin properties during heating/cooling, mechanisms of thermal damage, thermal pain, characterization and optimization of thermal treatment strategies, will be addressed in future studies.

Acknowledgments

This work is supported by the Overseas Research Studentship (ORS) and Overseas Trust Scholarship of Cambridge University, the National Natural Science Foundation of China (10328203, 10572111 and

10632060), the National 111 Project of China (B06024) and the National Basic Research Program of China (2006CB601202).

References

Abramson, D.I., 1967. Circulation in the Extremiries. Academic press, New York.

Agah, R., Gandjbakhche, A.H., Motamedi, M., Nossal, R., Bonner, R.F., 1996. Dynamics of temperature dependent optical properties of tissue: dependence on thermally induced alteration. IEEE Trans. Biomed. Eng. 43 (8), 839–846.

Aksan, A., McGrath, J.J., 2003. Thermomechanical analysis of soft-tissue thermotherapy. J. Biomech. Eng. 125 (5), 700–708.

Allain, J.C., Le Lous, M., Cohen-Salal, L., Bazin, S., Maroteaux, P., 1980. Isometric tensions developed during the hydrothermal swelling of rat skin. Connect. Tissue Res. 7, 127–133.

Arkin, H., Kimmel, E., Berman, A., Broday, D., 1991. Heat transfer properties of dry and wet furs of dairy cows. Trans. ASAE 34 (6), 2550–2558.

Arkin, H., Xu, L.X., Holmes, K.R., 1994. Recent developments in modeling heat transfer in blood perfused tissues. IEEE Trans. Biomed. Eng. 41 (2), 97–107.

Arnoczky, S.P., Aksan, A., 2000. Thermal modification of connective tissues: basic science considerations and clinical implications. J. Am. Acad. Orthop. Surg. 8 (5), 305–313.

Baek, S., Wells, P.B., Rajagopal, K.R., Humphrey, J.D., 2005. Heat-induced changes in the finite strain viscoelastic behavior of a collagenous tissue. J. Biomech. Eng. 127 (4), 580–586.

Bejan, A., 1990a. Optimum hair strand diameter for minimum free-convection heat transfer from a surface covered with hair. Int. J. Heat Mass Transfer 33 (1), 206–209.

Bejan, A., 1990b. Theory of heat transfer from a surface covered with hair. Trans. ASME, J. Heat Transfer 112, 662–667.

Bhowmick, S., Bischof, J.C., 1998. Supraphysiological thermal injury in dunning AT-1 prostate tumor cells. Adv. Heat Mass Transfer Biotechnol. ASME HTD-vol. 362/BED-vol. 40, 77–78.

Bosman, S., 1993. Heat-induced structural alterations in myocardium in relation to changing optical properties. Appl. Opt. 32 (4), 461–463.

Chachra, D., Gratzer, P.F., Pereira, C.A., Lee, J.M., 1996. Effect of applied uniaxial stress on rate and mechanical effects of cross-linking in tissue-derived biomaterials. Biomaterials 17 (19), 1865–1875.

Chae, Y., Aguilar, G., Lavernia, E.J., Wong, B.J., 2003. Characterization of temperature dependent mechanical behavior of cartilage. Lasers Surg. Med. 32 (4), 271–278.

Chao, K.K.H., Burden, M.A., Wong, B.J.F., 2001. Dynamic Changes in the Elastic Modulus of Lagomorph Nasal Septal Cartilage During Nd:YAG ($\lambda = 1.32\,\mu m$) Laser Irradiation. Society of Photo-Optical Instrumentation Engineers, San Jose, CA, pp. 247–254.

Charny, C.K., 1992. Mathematical models of bioheat transfer. Adv. Heat Transfer 22, 19–155.

Chato, J.C., 1980. Heat transfer to blood vessels. J. Biomech. Eng. Trans. ASME 102 (2), 110–118.

Chen, M.M., Holmes, K.R., 1980. Microvascular contributions in tissue heat transfer. Ann. NY Acad. Sci. 335, 137–150.

Chen, S.S., Humphrey, J.D., 1998. Heat-induced changes in the mechanics of a collagenous tissue: pseudoelastic behavior at 37 °C. J. Biomech. 31 (3), 211–216.

Chen, S.S., Wright, N.T., Humphrey, J.D., 1997. Heat-induced changes in the mechanics of a collagenous tissue: isothermal free shrinkage. J. Biomech. Eng. 119 (4), 372–378.

Chen, S.S., Wright, N.T., Humphrey, J.D., 1998a. Heat-induced changes in the mechanics of a collagenous tissue: isothermal, isotonic shrinkage. J. Biomech. Eng. 120 (3), 382–388.

Chen, S.S., Wright, N.T., Humphrey, J.D., 1998b. Phenomenological evolution equations for heat-induced shrinkage of a collagenous tissue. IEEE Trans. Biomed. Eng. 45 (10), 1234–1240.

Chvapil, M., Jensovsky, L., 1963. The shrinkage temperature of collagen fibres isolated from the tail tendons of rats of various ages and from different places of the same tendon. Gerontologia 1, 18–29.

Conrad, M.C., Anderson, J.L., Garrett, J.B., 1971. Chronic collateral growth after femoral artery occlusion in the dog. J. Appl. Physiol. 31, 550–555.

Crezee, J., Lagendijk, J.J., 1992. Temperature uniformity during hyperthermia: the impact of large vessels. Phys. Med. Biol. 37, 1321–1337.

Crezee, J., Mooibroek, J., Lagendijk, J.J., van Leeuwen, G.M., 1994. The theoretical and experimental evaluation of the heat balance in perfused tissue. Phys. Med. Biol. 39 (5), 813–832.

Dahan, S., Lagarde, J.M., Turlier, V., Courrech, L., Mordon, S., 2004. Treatment of neck lines and forehead rhytids with a nonablative 1540-nm Er:glass laser: a controlled clinical study combined with the measurement of the thickness and the mechanical properties of the skin. Dermatol. Surg. 30 (6), 872–879.

Davidson, J.M., Giro, M., Sutcliffe, M., Zoia, O., Quaglino, D., Liu, J.M., Perkett, E., Meryck, B., Broadley, K.N., Russell, S., Sephel, G.C., 1990. Regulation of elastin synthesis. In: Tamburro, A.M., Davidson, J.M. (Eds.), Elastin: Chemical and Biological Aspects. Congedo Editore, Galatina, Italy.

Davis, E.D., Doss, D.J., Humphrey, J.D., Wright, N.T., 2000. Effects of heat-induced damage on the radial component of thermal diffusivity of bovine aorta. J. Biomech. Eng. 122 (3), 283–286.

de Boer, J.F., Srinivas, S.M., Malekafzali, A., Chen, Z.P., Nelson, J.S., 1998. Imaging thermally damaged tissue by polarization sensitive optical coherence tomography. Opt. Express 3, 212–218.

Delalleau, A., Josse, G., Lagarde, J.M., Zahouani, H., Bergheau, J.M., 2006. Characterization of the mechanical properties of skin by inverse analysis combined with the indentation test. J. Biomech. 39 (9), 1603–1610.

Deng, Z.S., Liu, J., 2002. Analytical study on bioheat transfer problems with spatial or transient heating on skin surface or inside biological bodies. J. Biomech. Eng. 124 (6), 638–649.

Diaz, S., Lavemia, E., Wong, B.J.F., 2001. Mechanical Behavior of Cartilage During Laser Irradiation. Society of Photo-Optical Instrumentation Engineers, San Jose, CA, pp. 192–197.

Diller, K.R., Hayes, L.J., 1983. A finite element model of burn injury in blood-perfused skin. J. Biomech. Eng. Trans. ASME 105 (3), 300–307.

Diller, K.R., Pearce, J.A., 1999. Issues in modeling thermal alterations in tissues. Ann. NY Acad. Sci. 888, 153–164.

Duck, F.A., 1990. Physical Properties of Tissue: A Comprehensive Reference Book. Academic Press, New York.

Ebling, F., Eady, R., Leigh, I., 1992. Anatomy and organization of human skin. In: Champion, R.H., Burrington, J.L., Ebling, F.J.G. (Eds.), Textbook of Dermatology. Blackwell Scientific Publications, New York.

Elkins, W., Thomson, J.G., 1973. Instrumented thermal manikin. Acurex Corporation, Aerotherm Division Report AD-781, pp. 176.

Eroschenko, V.P., 2004. Di Fiores Atlas of Histology: With Functional Correlations. Lippincott Williams and Wilkins.

Flory, P.J., Garrett, R.R., 1958. Phase transition in collagen and gelatin systems. J. Am. Chem. Soc. 80, 4836–4845.

Fung, Y.C., 1990. Biomechanics: Motion, Flow, Stress, and Growth. Springer, New York.

Gebremedhin, K.G., Wu, B., 2001. A model of evaporative cooling of wet skin surface and fur layer. J. Therm. Biol. 26, 537–545.

Gebremedhin, K.G., Wu, B., 2002. Simulation of sensible and latent heat losses from wet-skin surface and fur layer. J. Therm. Biol. 27, 291–297.

Gordon, R.G., Roemer, R.B., Howath, S.M., 1976. A mathematical model of the human temperature regulatory system—transient cold exposure responses. IEEE Trans. Biomed. Eng. 23 (6), 434–444.

Green, D.M., Diller, K.R., 1978. Measurement of burn induced leakage of macromolecules in living tissue. Trans. ASME J. Biomech. Eng. 100, 153–158.

Hales, J.R.S., Iriki, M., Tsuchiya, K., Kozawa, E., 1978. Thermally induced cutaneous sympathetic activity related to blood flow through capillaries and arteriovenous anastomoses. Eur. J. Physiol. 375, 17–24.

Harris, J.L., Wells, P.B., Humphrey, J.D., 2003. Altered mechanical behavior of epicardium due to isothermal heating under biaxial isotonic loads. J. Biomech. Eng. 125, 381–388.

Hendriks, F.M., Brokken, D., Oomens, C.W., Bader, D.L., Baaijens, F.P., 2006. The relative contributions of different skin layers to the mechanical behavior of human skin in vivo using suction experiments. Med. Eng. Phys. 28 (3), 259–266.

Henriques, F.C., 1947. Study of thermal injuries V. The predictability and the significance of thermally induced rate processes leading to irreversible epidermal injury. Arch. Pathol. 43, 489–502.

Henriques, F.C., Moritz, A.R., 1947. Studies of thermal injury, 1. The conduction of heat to and through skin and the temperatures attained therein. A theoretical and an experimental investigation. Am. J. Pathol. 23, 531–549.

Humphrey, J.D., 2003. Continuum thermomechanics and the clinical treatment of disease and injury. Appl. Mech. Rev. 56 (2), 231–260.

Jacques, S.L., 2006. Ratio of entropy to enthalpy in thermal transitions in biological tissues. J. Biomed. Opt. 11 (4), 041108.

James, N.C., Richard, A.M., 1996. Neurobiology of Nociceptors. Oxford University Press, Oxford.

Joyner, M.J., Dietz, N.M., 1997. Nitric oxide and vasodilation in human limbs. J. Appl. Physiol. 83, 1785–1796.

Jun, J.H., Harris, J.L., Humphrey, J.D., Rastegar, S., 2003. Effect of thermal damage and biaxial loading on the optical properties of a collagenous tissue. J. Biomech. Eng. 125 (4), 540–548.

Khaled, A.R.A., Vafai, K., 2003. The role of porous media in modeling flow and heat transfer in biological tissues. Int. J. Heat Mass Transfer 46 (26), 4989–5003.

Kollar, L.P., Springer, G.S., 2003. Mechanics of Composite Structure. Cambridge University Press, Cambridge.

Kondo, E., Yasuda, K., Kitamura, N., Kudoh, T., Minami, A., Tohyama, H., 2005. The effect of electrothermal shrinkage on the biomechanical properties of the anterior cruciate ligament: an experimental study. Arthroscopy 21 (4), 448–456.

L'Etang, A., Huang, Z., Yang, D., 2006. Simulation of laser ultrasonic surface wave dispersion in a multilayered skin model. Conference Proceedings of the IEEE Engineering in Medicine and Biology Society, vol. 1, pp. 5072–5075.

Le Lous, M., Flandin, F., Herbage, D., Allain, J.-C., 1982. Influence of collagen denaturation on the chemorheological properties of skin assessed by differential scanning calorimetry and hydrothermal isometric tension measurement. Biochim. Biophys. Acta (BBA)—Gen. Subjects 717 (2), 295–300.

Le Lous, M., Cohen-Solal, L., Allain, J.C., Bonaventure, J., Maroteaux, P., 1985. Age related evolution of stable collagen reticulation in human skin. Connect. Tissue Res. 13, 145–155.

Lemons, D.E., Chien, S., Crawshaw, L.I., Weinbaum, S., Jiji, L.M., 1987. Significance of vessel size and type in vascular heat transfer. Am. J. Physiol. 253 (1 Pt 2), R128–R135.

Lennox, F.G., 1949. Shrinkage of collagen. Biochim. Biophys. Acta 3, 170–187.

Lin, S.J., Lo, W., Tan, H.Y., Chan, J.Y., Chen, W.L., Wang, S.H., Sun, Y., Lin, W.C., Chen, J.S., Hsu, C.J., Tjiu, J.W., Yu, H.S., Jee, S.H., Dong, C.Y., 2006. Prediction of heat-induced collagen shrinkage by use of second harmonic generation microscopy. J. Biomed. Opt. 11 (3), 34020.

Lin, W., Motamedi, M.M., Welch, A.J., 1996. Dynamics of tissue optics during laser heating of turbid media. Appl. Opt. 35 (19), 3413–3420.

Liu, J., Wang, C., 1997. Bioheat Transfer. Science Press.
Lubashevsky, I.A., Gafiychuk, V.V., 2004. Mathematical description of the heat transfer in living tissue (Part I). adap-org/9911001.
Magnenat-Thalmann, N., Kalra, P., Leveque, J.L., Bazin, R., Batisse, D., Querleux, B., 2002. A computational skin model: fold and wrinkle formation. IEEE Trans. Inf. Technol. Biomed. 6 (4), 317–323.
McCleskey, E.W., Gold, M.S., 1999. Ion channels of nociception. Annu. Rev. Physiol. 61, 835–856.
McHugh, A.A., Fowlkes, B.J., Maevsky, E.I., Smith Jr., D.J., Rodriguez, J.L., Garner, W.L., 1997. Biomechanical alterations in normal skin and hypertrophic scar after thermal injury. J. Burn Care Rehabil. 18 (2), 104–108.
Melling, M., Pfeiler, W., Karimian-Teherani, D., Schnallinger, M., Sobal, G., Zangerle, C., Menzel, E.J., 2000. Differential scanning calorimetry, biochemical, and biomechanical analysis of human skin from individuals with diabetes mellitus. Anat. Rec. 59, 327–333.
Miles, C.A., 1993. Kinetics of collagen denaturation in mammalian lens capsules studied by differential scanning calorimetry. Int. J. Biol. Macromol. 15 (5), 265–271.
Miles, C.A., Bailey, A.J., 2001. Thermally labile domains in the collagen molecule. Micron 32 (3), 325–332.
Moritz, A.R., Henriques, F.C., 1947. Study of thermal injuries II. The relative importance of time and source temperature in the causation of cutaneous burns. Am. J. Pathol. 23, 695–720.
Ng, E.Y., Chua, L.T., 2000. Mesh-independent prediction of skin burns injury. J. Med. Eng. Technol. 24 (6), 255–261.
Ozisik, M.N., 1993. Heat Conduction. Wiley, New York.
Pearce, J., Thomsen, S., Vijverberg, H., McMurray, T., 1993. Kinetics of birefringence changes in thermally coagulated rat skin collagen. Proc. SPIE, 180–186.
Pennes, H.H., 1948. Analysis of tissue and arterial blood temperatures in the resting human forearm. J. Appl. Physiology 1, 93–122.
Pierce, M.C., Sheridan, R.L., Park, B.H., Cense, B., De Boer, J.F., 2004. Collagen denaturation can be quantified in burned human skin using polarization-sensitive optical coherence tomography. Burns 30, 511–517.
Reay, D.A., Thiele, F.A.J., 1977. Heat pipe theory applied to a biological system. Quantification of the role of the resting eccrine sweat gland in thermoregulation. J. Theor. Biol. 64, 789–803.
Reihsner, R., Balogh, B., Menzel, E.J., 1995. Two-dimensional elastic properties of human skin in terms of an incremental model at the in vivo configuration. Med. Eng. Phys. 17 (4), 304–313.
Reihsner, R., Melling, M., Pfeiler, W., Menzel, E.J., 2000. Alterations of biochemical and two-dimensional biomechanical properties of human skin in diabetes mellitus as compared to effects of in vitro non-enzymatic glycation. Clin. Biomech. 15, 379–386.
Reuck, A.V.S., Knight, J., 1966. Touch, Heat and Pain. Churchill Ltd.
Rigal, J.D., Leveque, J., 1985. In vivo measurement of the stratum corneum elasticity. Bioeng. Skin 1, 13–23.
Roetzel, W., Xuan, Y., 1998. Transient response of the human limb to an external stimulus. Int. J. Heat Mass Transfer 41 (1), 229–239.
Schwartz, G.G., Rosenblum, L.A., 1981. Allometry of primate hair density and the evolution of human hairlessness. Am. J. Phys. Anthropol 55 (1), 9–12.
Sejrsen, P., 1972. Measurement of cutaneous blood flow by freely diffusible radioactive isotopes. Dan. Med. Bull. 18, 1–38.
Srinivas, S.M., deBoer, J.F., Park, H., Keikhanzadeh, K., Huang, H.E., Zhang, J., Jung, W.Q., Chen, Z., Nelson, J.S., 2004. Determination of burn depth by polarization-sensitive optical coherence tomography. J. Biomed. Opt. 9 (1), 207–212.
Stanczyk, M., Telega, J.J., 2002. Modelling of heat transfer in biomechanics—a review. Part I. Soft tissues. Acta Bioeng. Biomech. 4 (1), 31–61.
Thomsen, S., 1991. Pathologic analysis of photothermal and photomechanical effects of laser–tissue interactions. Photochem. Photobiol. 53 (6), 825–835.
Torvi, D.A., Dale, J.D., 1994. A finite element model of skin subjected to a flash fire. J. Biomech. Eng. 116 (3), 250–255.
Van Hees, J., Gybels, J., 1981. C nociceptor activity in human nerve during painful and non painful skin stimulation. J. Neurol. Neurosurg. Psychiatry 44 (7), 600–607.
Weinbaum, S., Jiji, L.M., Lemons, D.E., 1984. Theory and experiment for the effect of vascular microstructure on surface tissue heat transfer—Part I: anatomical foundation and model conceptualization. J. Biomech. Eng. 106 (4), 321–330.
Wells, P.B., Harris, J.L., Humphrey, J.D., 2004. Altered mechanical behavior of epicardium under isothermal biaxial loading. J. Biomech. Eng. 126, 492–497.
Whitton, J.T., Everall, J.D., 1973. The thickness of the epidermis. Br. J. Dermatol. 89, 467–476.
Wright, N.T., 2003. On a relationship between the Arrhenius parameters from thermal damage studies. J. Biomech. Eng. 125, 300–304.
Xu, Y., Hua, T.C., Sun, D.W., Zhou, G.Y., Xu, F., 2007. Effects of freezing rates and dimethyl sulfoxide concentrations on thermal expansion of rabbit aorta during freezing phase change as measured by thermo mechanical analysis. J. Biomech. 40 (14), 3201–3206.
Yen, A., Braverman, I.M., 1976. Ultrastructure of the human dermal microcirculation: the horizontal plexus of the papillary dermis. J. Invest. Dermatol. 66 (3), 31–142.
Young, G.S., 1998. Thermodynamic characterization of skin, hide and similar materials composed of fibrous collagen. Stud. Conserv. 43 (2), 65–79.